CANADIAN THESES

THÈSES CANADIENNES

NOTICE

The quality of this microfiche is heavily dependent upon the quality of the original thesis submitted for microfilming. Every effort has been made to ensure the highest quality of reproduction possible.

If pages are missing, contact the university which granted the degree.

Some pages may have indistinct print especially if the original pages were typed with a poor typewriter ribbon or if the university sent us an inferior photocopy.

Previously copyrighted materials (journal articles, published tests, etc.) are not filmed.

Reproduction in full or in part of this film is governed by the Canadian Copyright Act, R.S.C. 1970, c. C-30.

AVIS

La qualité de cette microfiche dépend grandement de la qualité de la thèse soumise au microfilmage. Nous avons tout fait pour assurer une qualité supérieure de reproduction.

S'il manque des pages, veuillez communiquer avec l'université qui a conféré le grade.

La qualité d'impression de certaines pages peut laisser à désirer, surtout si les pages originales ont été dactylographiées à l'aide d'un ruban usé ou si l'université nous a fait parvenir une photocopie de qualité inférieure.

Les documents qui font déjà l'objet d'un droit d'auteur (articles de revue, examens publiés, etc.) ne sont pas microfilmés.

La reproduction, même partielle, de ce microfilm est soumise à la Loi canadienne sur le droit d'auteur, SRC 1970, c. C-30.

THIS DISSERTATION HAS BEEN MICROFILMED EXACTLY AS RECEIVED

LA THÈSE A ÉTÉ MICROFILMÉE TELLE QUE NOUS L'AVONS REÇUE

THE UNIVERSITY OF ALBERTA

APPLICATION OF ITERATIVE INVERSION TECHNIQUES IN CRUSTAL SEISMOLOGY

by

MOSTAFA SHAHRIAR

A THESIS

SUBMITTED TO THE FACULTY OF GRADUATE STUDIES AND RESEARCH

IN PARTIAL FULFILMENT OF THE REQUIREMENTS FOR THE DEGREE

OF DOCTOR OF PHILOSOPHY

IN

GEOPHYSICS

DEPARTMENT OF PHYSICS

EDMONTON, ALBERTA

SPRING 1987

ISBN 0-315-37673-2

THE UNIVERSITY OF ALBERTA

RELEASE FORM

NAME OF AUTHOR MOSTAFA SHAHRIAR

TITLE OF THESIS APPLICATION OF ITERATIVE INVERSION TECHNIQUES IN CRUSTAL SEISMOLOGY

DEGREE FOR WHICH THESIS WAS PRESENTED DOCTOR OF PHILOSOPHY

YEAR THIS DEGREE GRANTED SPRING 1987

Permission is hereby granted to THE UNIVERSITY OF ALBERTA LIBRARY to reproduce single copies of this thesis and to lend or sell such copies for private, scholarly or scientific research purposes only.

The author reserves other publication rights, and neither the thesis nor extensive extracts from it may be printed or otherwise reproduced without the author's written permission.

(SIGNED) Mshahriar .....

PERMANENT ADDRESS:

54 Circular Road
Dhanmondi, Dhaka 1205
Bangladesh

DATED November 13, 1986.

THE UNIVERSITY OF ALBERTA

FACULTY OF GRADUATE STUDIES AND RESEARCH

The undersigned certify that they have read, and recommend to the Faculty of Graduate Studies and Research, for acceptance, a thesis entitled APPLICATION OF ITERATIVE INVERSION TECHNIQUES IN CRUSTAL SEISMOLOGY submitted by MOSTAFA SHAHRIAR in partial fulfilment of the requirements for the degree of DOCTOR OF PHILOSOPHY in GEOPHYSICS.

.....

Supervisor

.....

.....

.....

.....

External Examiner

Date. November 13, 1986.....

To our beloved mother who

sacrificed her life for us

ABSTRACT

An efficient linearized inversion program using Asymptotic Ray theory (ART) and the least squares technique is presented. Seismic amplitude and travel time data are used to derive earth models of simple structure. It is demonstrated that simultaneous use of both kinematic and dynamic data results in a better resolution for the model parameters and the ability to extract additional information such as density and shear wave velocities from the vertical component seismogram alone. The program has been tested for multiple layered and horizontally structured earth models using head waves, primary and multiple reflections including low velocities and multiple shot points.

Only kinematic data are used to study relatively complex models. Inversion of synthetic and field data in terms of curved and arbitrarily dipping models shows that the two dimensional attitude of crustal boundaries can be determined from secondary P arrivals. These results may be considered as an important first step towards a unified approach where both travel time and amplitude data can be used for modeling of realistic structures.

ACKNOWLEDGEMENTS

I would like to thank my supervisors Dr. G. L. Cumming and Dr. F. Hron for their continued assistance throughout the study. Dr. Hron is to be specially thanked for suggesting the topic of amplitude inversion.

I thank my wife Sultana for her loving support during the ups and downs of this project.

I am also grateful to Mrs. Eva Cumming for caring so much about us.

During the course of this study, I received financial support from the Department of Physics, University of Alberta.

Table of Contents

List of Tables

List of Figures

1. INTRODUCTION

Application of iterative matrix inversion techniques has been of use in many geophysical inverse problems. Many earth scientists have used this approach successfully to invert data of various physical and statistical character (Braile, 1973; Aki and Lee, 1976; Vignersesse, 1978; Hoversten et al., 1982). Up to now a large number of new areas of application have been explored in the field of seismology (Garmany, 1982; Ursin and Zheng, 1985; Ivansson, 1985; Gersztenkorn et al., 1986; McNutt and Jacob, 1986). It is expected that past results from the numerous successful inversion studies employing this method will encourage many more newer applications in the coming years. The programs developed in the recent years show varied computational efficiency and accuracy of results. Often the efficiency of these programs is determined in terms of the computer costs involved. An inexpensive program largely depends on how quickly the forward model is calculated and how many iterations are required for convergence. In this thesis an efficient inversion program is developed to investigate new applications in the field of crustal seismology.

In seismology most of the previous studies involved inversion of travel time data in terms of various simple as well as complex earth models (Braile, 1973; Aki and Lee, 1976; Crosson, 1976; Benz and Smith, 1984; Chiu et al.,

1985). However few attempts have been made to use this technique for the direct inversion of amplitude data. Most often, use of dynamic information has been carried out in terms of visual waveform matching using synthetic seismograms. Visual fitting of observed data needs considerable personal attention by the seismologist. Moreover, accuracy is limited by the extent of individual perception. On the other hand automated matching using the recently developed tomography method (Culter et al., 1984; Chiu et al., 1985; Nakanishi, 1985) is gaining popularity. Most tomographic methods use kinematic data for inversion. Automated amplitude matching has not been attempted in crustal seismology as yet. This is partly because of the complexity involved in suitable parameterization of the amplitude function in terms of the earth structure and also to a considerable extent because of enormous computer time usually involved in the forward ray tracing process.

The inversion program used in this study uses parameterization and inversion of the amplitude data using Asymptotic Ray Theory (ART). The analysis yields earth structure in terms of density, compressional and shear wave velocities for isotropic, homogeneous and horizontally layered models. The program has been used for both head wave and reflection amplitudes including multiple reflection arrivals. Excellent numerical results indicate the potential of this method for further application to complex geological structures.

Computation of the response at specific geophone location has been accomplished using a two-point ray tracing algorithm. All the calculations have been performed using both analytical and numerical approaches. It has been found that the analytical computations are more accurate (as expected) and involve less computation time. A few iterations (typically 3 to 6 iterations) have been enough to obtain an acceptable fit to the observations in terms of a root mean squared (RMS) deviation criterion.

One advantage of our technique is that both kinematic and dynamic information may be used simultaneously without data modification. It has been found that combined use of both types of data results in better resolution of the model parameters. Moreover, since density, P and S wave velocities are computed simultaneously, a quantitative estimation of the elastic properties of the medium under study is also possible using this method. It has been demonstrated that the program can be used for multiple layers and multiple shot points. Converted phases may be incorporated easily with only slight modifications. It has also been found that this method is successful in detecting low velocity zones and multiple arrivals which have been always a difficult problem for kinematic interpretation methods.

Care must be taken in the application of this method for amplitudes near the critical region, especially with low frequency signals. This is due to the fact that the plane

wave reflection coefficient which is used for the amplitude computation in ART exhibits an infinite derivative in the vicinity of the critical angle. One is able to overcome this problem if a suitable high frequency approximation such as the Weber function approximation of Marks and Hron (1979) is used.

The program has been designed for numerical modeling as well as interpretation of the field amplitude data. Conventional seismic records often fail to represent the true amplitudes due to lack of proper control over the geophone gains and also because of variation in the geophone to ground coupling. Therefore for the present, use of the program has been restricted primarily to synthetic amplitudes in order to test the range of applicability of the method.

Chapters 4 and 5 are mainly devoted to the investigation of 2-D characteristics of reflecting boundaries including curved interfaces and plane boundaries with arbitrary dips. It is shown that the program may be used successfully to detect the 2-D nature of crustal structures especially the Moho interface. Synthetic and field examples are used to invert crustal PmP arrivals in terms of the 2-D Moho boundary. Simple two layer models are used to emphasize the main result. Structures with additional number of layers or other complexity such as velocity gradient, curvature, dip, and or suddenly vanishing horizons which may be adequately described by ART, may be

incorporated with suitable ray tracing scheme included in the forward model.

2. THE INVERSE METHOD

If the internal structure and physical properties of the earth were precisely known the magnitude of any particular geophysical measurement taken at the earth's surface could be predicted uniquely. Thus, for example, it would be possible to predict the travel time of a seismic wave reflected from any buried interface or to predict the gravitational and magnetic fields at the surface due to a known structure inside the earth. In geophysical surveying the problem is of opposite nature and usually the requirement is to deduce some aspect of the earth's interior on the basis of measurements taken at or near the earth's surface. The former type is known as the direct problem while the later is called the inverse problem.

In the inversion process usually a finite number of observed data are fitted to the response of an idealized model. The model is perturbed until the response closely matches the essential features of the observation. The model is represented in terms of a set of mathematical relations involving desired physical properties of the medium. These equations contain a finite number of independent variables (e.g., velocity, density, thickness etc) called the model parameters Xi The dependent variable is termed the response function or the model response. Let us consider an example to explain these terms. The travel time curve for reflected body waves from a horizontal

interface located at depth H below the surface is given by

$$T_i = [D_i^2 + 4H^2]^{1/2}/V \qquad (1)$$

where, i=1,2,3....m; m being the number of geophones that record the reflection arrivals. For this particular model (figure-2.1) we have 2 model parameters; namely, the thickness H and the velocity V of the upper medium. D_i is a known constant which represents the horizontal distance of the ith geophone from the source location. It is obvious from equation (1) that the travel time T_i at location D_i depends on the independent parameters H and V i.e., $T_i = f_i(H,V)$. Generally the model response f_i is a nonlinear function of the model parameters. Calculations may be performed using methods of linear algebra if we linearize the problem using a first order Taylor series expansion of the final response f_i about an initial starting response f_i^0

$$f_i = f_i^0 + \sum_{j=1}^{n} \partial f_i/\partial X_j|_0^b \, (X_j - X_j^0) \qquad (2)$$

where,

$f_i = f_i(x_1,....x_n)$ = final model response at ith observation point.

$f_i^0 = f_i(x_i^0,....x_n^0)$ = initial response at ith observation point.

X_j = final value of jth model parameter.

X_j^0 = initial estimate of jth model parameter.

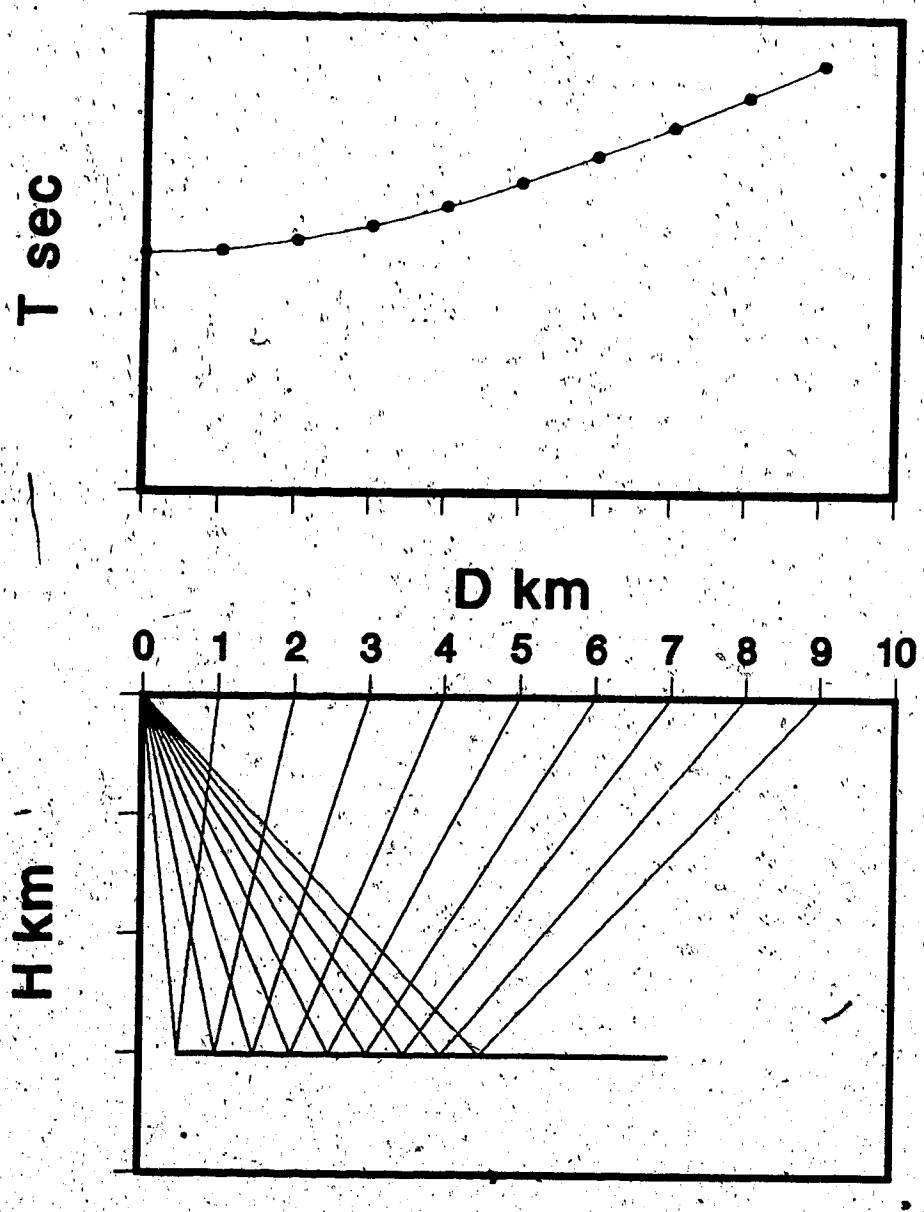

Figure 2.1 Reflection travel time curve for a two-layer homogeneous velocity model (receiver locations are indicated by numerals 1, 2,.. etc.)

n = total number of model variables.

One should, however, be cautious about using the term "linearization". It is virtually impossible to linearize a truly non-linear problem. What equation (2) does mean is that if the starting response f^0 is sufficiently close to the exact response f then equation (2) is only approximately true in the close vicinity of the exact solution. In other words we have assumed a localized linearization of the problem about the exact solution. All the calculations and the convergence attempts must be restricted within the limit of the local quasilinear part. Otherwise expectation for a realistic convergent solution would be in vain.

Generally we assume that the travel time picking error is of the order of 5 to 10 milliseconds. When the RMS error for travel time defined as

$$RMS = \sum_{i=1}^{m} [T_c(i) - T_o(i)]^{1/2}/m$$

is computed from the difference of the calculated and observed travel times (T_c and T_o respectively), we are directly considering the noise in the data and the inability of the model to describe the observation accurately. Therefore, we do not want the RMS value to exceed the usual travel time picking error. In other words the computed model may be cosidered as a smoothed version of the actual model the extent of smoothing being limited by the

uncertainty in the data. Therefore a close fit means reducing the noise RMS (by iterating) as far as possible so that our inability of model formulation may not exceed the actual travel time reading error.

In most geophysical inverse problems it has been observed that there are always more than one solution corresponding to different localized linear zones. Therefore it is important to distinguish between realistic and nonfeasible solutions. In most cases the interpreter has a priori knowledge of the approximate solution probably from previous studies or other sources such as well logs and magnetic studies in the same area. A starting response called the initial estimate is obtained from the approximate solution by forward model calculation. For m number of observation points equation (2) constructs an array of numbers which can be expressed in the matrix form

$$|A||\Delta X| = |\Delta B| \qquad (3)$$

where,

$A_{ij} = (\partial f_i / \partial X_j)|_0$

$i=1,2....m;\ j=1,2,....n.$

$\Delta X = X - X^0$

$\Delta B = f - f^0$

The residual vector ΔB contains the difference between the final and initial responses. For our purpose ΔB represents the difference between the observed and initially computed

travel times or amplitudes. To further illustrate the method of computation of matrix elements A_{ij} we consider the example given in equation (1) with two model parameters (i.e., n=2) and select $X_1 = V$ and $X_2 = H$. For three observation points (m=3) the elements of the 3×2 matrix **A** using equation (1) are given by

$$A_{11} = \frac{\partial f_1}{\partial X_1} = \frac{\partial T_1}{\partial V} = \frac{-T_1}{V}$$

$$A_{21} = \frac{-T_2}{V}$$

$$A_{31} = \frac{-T_3}{V} \qquad (4)$$

$$A_{12} = \frac{-4HT_1}{4H^2+D_1^2}$$

$$A_{22} = \frac{4HT_2}{4H^2+D_2^2}$$

$$A_{32} = \frac{4HT_3}{4H^2+D_3^2}$$

where T_1, T_2 and T_3 represent travel times at observation points 1, 2 and 3 respectively. It is clear from (3) that the correction vector ΔX can be obtained from

$$|\Delta X| = |A|^{-1}|\Delta B| \qquad (5)$$

so that the final improved vector is

$$|X| = |X^0| + |A|^{-1}|\Delta B| \qquad (6)$$

If X^0 differs from X significantly, it may be necessary to iterate towards X until ΔB is small. For a truly linear system this is a one step iterative process. For the nonlinear case several iterations may be required before convergence occurs. In any case linearity usually holds in the vicinity of the true solution and the error estimates and confidence region estimations based on the linearity assumption apply. In equation (5) the exact inverse A^{-1} exists only if A is a square matrix. For most geophysical problems there are more observations than model parameters causing A to be a rectangular matrix. Therefore if a solution exists, it should be determined by a least squares method.

It may appear that it is possible to reformulate the overdetermined system into several well determined systems each having equal number of data points and model variables. There is one major problem to this approach. Although we have a seemingly overdetermined system we are actually dealing with an underdetermined system. This is because many observation points do not reveal any new information. In other words, taking more and more observations will not necessarily illuminate the entire region under consideration. Also there may be numerous contributions to the observation from unknown sources. What we consider is just a simplified picture (or model) of the actual earth

structure. Generally resolution (formal definition introduced later in this chapter) increases with addition of data points up to a certain point after which further addition of data becomes ineffective. However, it is possible to identify the the data points contributing independent information by computing the Information Density Matrix given in equation (31).

If however, we divide the whole data set into several blocks creating several seemingly well determined systems, it is possible to run the computer program for inversion without generating any error. But this would merely indicate that we want to force a solution in terms of apparently well determined systems which are actually underdetermined. Obviously an attempt to get a solution based on this approach may generate poorly resolved model parameters. It may happen that some blocks will have well determined parameters others will not. It may also happen that every block will have parameters only partially resolved because of inherent underdeterminancy.

To obtain a least squares solution, let us consider the error E for each data set

$$|E| = |A||\Delta X| - |\Delta B| \qquad (7)$$

Minimization of the squared norm E^tE (^{t} means transpose) with respect to the solution vector ΔX leads to a set of normal equations of the form (Appendix-A5)

$$|\Delta X| = |A^tA|^{-1}|A^t\Delta B| \qquad (8)$$

Solution vector X may be obtained using equations (5), (6) and (8) but formation of $(A^tA)^{-1}$ and $(A^t\Delta B)$ involves numerical inaccuracies due to instability caused by the ill conditioning of the matrix A and the inaccuracies may be particularly troublesome for large values of m and n. This problem can be avoided following Lanczos (1961) and Golub and Reinsch (1970) in which the matrix A is factored into three product matrices

$$|A| = |U||\Lambda||V|^t \qquad (9)$$

where, U, Λ, and V are m×m, m×n and n×n array spaces. U and V are semiorthogonal matrices whose columns form respectively the basis vectors for the data space and the solution space activated by the operator A. The column vectors u_i and v_i of U and V respectively satisfy

$$AA^tu_i = \lambda_i^2 u_i$$
$$A^tAv_i = \lambda_i^2 v_i \qquad (10)$$

where,

$i = 1, 2, 3 \ldots n<m.$

$\lambda_{n+1} = \lambda_{n+2} = \ldots = \lambda_m = 0.$

λ_i^2's are the eigenvalues of the hermitian matrix AA^t. By convention the sets of eigenvalues are ordered in decreasing

size and are together called the eigenvalue spectrum. Λ is the diagonal matrix having the square-root of the eigenvalues of $\mathbf{AA}^t$. The method of matrix factorization given by equation (9) is called the singular value decomposition (SVD). Operator **A** describes a mapping from n-dimensional parameter space to m-dimensional observation space. Semiorthogonal properties of **U** and V are given by

$$\begin{aligned} \mathbf{U}_k^t\mathbf{U}_k &= \mathbf{I}_k \\ \mathbf{V}_k^t\mathbf{V}_k &= \mathbf{I}_k \end{aligned} \tag{11}$$

where $\mathbf{U}_k$ is the orthogonal equivalent of matrix **U** retaining k nonzero eigenvalues and $\mathbf{I}_k$ is k×k identity matrix. k is referred to as the rank of the matrix **A**. In terms of the decomposed matrices **U**, Λ, and V the inverse operator $\mathbf{A}^{-1}$ can be written as

$$|\mathbf{A}|^{-1} = |\mathbf{V}||\Lambda|^{-1}|\mathbf{U}|^t \tag{12}$$

which is called the Natural or Generalized or Lanczos inverse of **A**. Since the inverse of the diagonal matrix Λ can be obtained from the reciprocal of its diagonal elements such as

$$|\Lambda|^{-1} = \begin{vmatrix} \lambda_{11}^{-1} & & & \\ & \lambda_{22}^{-1} & & \mathbf{0} \\ & & \ddots & \\ & \mathbf{0} & & \lambda_{kk}^{-1} \end{vmatrix} \tag{13}$$

where λ represents the eigenvalues of **A** and k is the rank of matrix **A**, construction of $\mathbf{A}^{-1}$ from **U**, Λ^{-1} and V becomes easier involving only simple matrix multiplications. However, it is also obvious that Λ^{-1} and consequently $\mathbf{A}^{-1}$ cease to exist when any of the eigenvalues in Λ becomes zero. This is always a possibility due to insufficient information in the observation space. Therefore if it is not possible to increase the number of observations it may be convenient to eliminate all zero or near zero eigenvalues. For k nonzero eigenvalues

$$| \underset{nxm}{\mathbf{A}} |^{-1} = | \underset{nxk}{\mathbf{V}} | | \underset{kxk}{\Lambda} |^{-1} | \underset{kxm}{\mathbf{U}} |^{t} \qquad (14)$$

The question may arise as to how small is the magnitude of the nonzero eigenvalue that is to be suppressed. This may be decided from a threshold value determined from the estimate of the relative error involved in the input data. For example if the data are accurate to three significant figures then the relatve error estimation may be chosen to be 10^{-3}. If the data are regarded as exact then the relative error estimation must reflect the round-off error expected in the computations such as in the SVD algorithm itself which is approximately n times the machine epsilon. The threshold value for error tolerance (Forsythe et al., 1977) is then obtained from

$$\text{TOL} = (\text{relative error}) \times (\text{largest eigenvalue}) \qquad (15)$$

Singular values smaller than this number are dropped from the eigenvalue spectrum. Since, for small eigenvalues of **A**,

the random errors in the data tend to cause more fluctuations in the solution, additional measures are taken to suppress undesirable effects by using the damping criteria (Levenberg, 1944; Marquardt, 1961). In this process a positive constant β is added to the diagonal elements of the matrix Λ such that

$$| \underset{n\times m}{\mathbf{A}} |^{-1} = | \underset{n\times k}{\mathbf{V}} | | \underset{k\times k}{\Lambda} | | \underset{k\times k}{\Lambda^2 + \beta^2 \mathbf{I}} |^{-1} | \underset{k\times m}{\mathbf{U}} |^{t} \qquad (16)$$

where β is called the damping factor. Combining (5) and (16) we get (Appendix-A5).

$$| \underset{n\times 1}{\Delta \mathbf{X}} | = | \underset{n\times k}{\mathbf{V}} | | \underset{k\times k}{\Lambda} | | \underset{k\times k}{\Lambda^2 + \beta^2 \mathbf{I}} |^{-1} | \underset{k\times m}{\mathbf{U}} |^{t} | \underset{m\times 1}{\Delta \mathbf{B}} | \qquad (17)$$

β effectively adds a dc level to the eigenvalues of **A** so that none of them may vanish therefore eliminating a possible division by zero. However if β is sufficiently large, Δ**X** is small and contributes very little towards a progressive solution given by equation (17). Therefore an optimum value for β must be found experimentally. The properties of β have been described in Lines and Treitel (1984). Usually it controls the stability and number of iterations and depends on the degree of underdeterminancy of the system of equations, the nonlinearity of the problem and the noise level of the observed data. A good estimate of β is given by weighting the residuals by the reciprocal of the variances of the observations (Crosson, 1976). This leads to a normally distributed random variable with unit variance. Aki and Lee (1976) used a weight proportional to the ratio of the variance of the data and the variance of

the estimated solution. Hoerl et al. (1975) have suggested that an appropriate choice for β is

$$\beta = n\sigma_d^2/X^tX \qquad (18)$$

where,

σ_d = standard deviation for the data set.

n = the number of degrees of freedom.

X^tX = product of solution vector and its transpose computed from undamped least squares method.

In addition to the damping, a scaling factor may also be used to avoid ill conditioning caused by different scales in which the model parameters are expressed.

2.1 Resolution and Errors:

A good match to the observed data does not always guarantee the best solution. Study of the reliability of the derived model and the errors associated with the calculated model variables give a better understanding about the nature of the solution. The matrix inversion process provides a means to quantify the degree of nonuniqueness inherent in the system by estimating the resolution and variances of the model parameters (Backus and Gilbert, 1967). From equation (5)

$$|\Delta X| = |A|^{-1}|\Delta B| \qquad (5a)$$

If the approximate inverse of matrix A is given by A_a^{-1} then the approximate solution may be written as

$$|\Delta X_a| = |A_a|^{-1}|\Delta B| \tag{19}$$

From equations (5a) and (19) we get

$$|\Delta X_a| = |A_a|^{-1}|A||\Delta X| \tag{20}$$

which expresses the computed solution ΔX_a as weighted average of the true solution with weights given by the row vectors of the matrix $A_a^{-1}A$. This weight matrix is called the resolution matrix R

$$|R| = |A_a^{-1}A| \tag{21}$$

If R is an identity matrix I, the resolution is perfect and the computed approximate solution is equal to the true solution. This means that a unique solution has been obtained in the mathematical sense. Fractional values for the diagonal elements of R mean that there are significant off-diagonal elements indicating a possible distortion in the computed final result. The solution obtained only represents a smoothed one over the spread around the diagonal. Therefore the elements of the matrix R should be carefully examined to detect nonuniqueness in the solution. Hence the usual practice has been to quote the diagonal element of R which corresponds to the particular element of the computed solution.

Since ΔB represents the difference between the computed and predicted amplitude or travel time we may consider ΔB to represent the error of the data. It is then possible to express the error in the computed solution in terms of the

data error by computing the covariance C of the solution vector as follows

$$|C| = \langle \Delta X_a \Delta \tilde{X}_a \rangle = \langle A_a^{-1} \Delta B \Delta \tilde{B} \tilde{A}_a^{-1} \rangle \approx A_a^{-1} \langle \Delta B \Delta \tilde{B} \rangle \tilde{A}_a^{-1} \qquad (22)$$

If the data vectors are statistically independent and share the same variance σ_d^2 we can write

$$|C| = \langle \Delta X_a \Delta \tilde{X}_a \rangle = \sigma_d^2 |A_a \tilde{A}_a|^{-1} \qquad (23)$$

where $\tilde{}$ means conjugate transpose and $\sigma_d^2 = \langle \Delta B \Delta \tilde{B} \rangle$ is called the data variance. When we use the SVD in the expressions for resolution R and covariance C (i.e., using $A = U\Lambda V^t$ and $A_a^{-1} = V\Lambda^{-1}U^t$, since both A and A_a^{-1} share the same component matrices) we can write from equation (21)

$$\begin{aligned} |R| &= |A_a^{-1}A| \\ &= |V||\Lambda|^{-1}|U|^t|U||\Lambda||V|^t \\ &= |V||\Lambda|^{-1}|\Lambda||V|^t \qquad (24) \\ &= |V||V|^t \qquad (25) \end{aligned}$$

Including the damping effect and retaining only k nonzero singular values the expressions for R and C become

$$\left| \underset{nxn}{R} \right| = \left| \underset{nxk}{V} \right| \left| \underset{kxk}{\Lambda} \right|^2 \left| \underset{kxk}{\Lambda^2} + \beta^2 \underset{kxk}{I} \right|^{-1} \left| \underset{kxn}{V} \right|^t \qquad (26)$$

$$\left| \underset{nxn}{C} \right| = \sigma_d^2 \left| \underset{nxk}{V} \right| \left| \underset{kxk}{\Lambda} \right|^2 \left| \underset{kxk}{\Lambda^2} + \beta^2 \underset{kxk}{I} \right|^{-2} \left| \underset{kxn}{V} \right|^t \qquad (27)$$

An estimate of σ_d^2 can be obtained from the sum of the

squared residuals divided by the number of degrees of freedom such as

$$\sigma_d^2 = \sum_{i=1}^{m} (\Delta B - A\Delta X)^2/(m-n) \qquad (28)$$

It is clear from equations (26) and (27) that β reduces the error of the model parameters by sacrificing the resolution. This leads us to consider a reasonable trade-off between the resolution and the covariance (Backus and Gilbert, 1967).

Let us now consider the resolution in the data space. The observed data vector ΔB can be related to the computed (i.e., predicted) vector ΔB_a as follows

$$|\Delta B_a| = |A||\Delta X_a|$$

Using equation (19)

$$|\Delta B_a| = |AA_a^{-1}||\Delta B| \qquad (29)$$

Applying SVD for k nonzero singular values

$$|\Delta B_a| = |U||U|^t|\Delta B| \qquad (30)$$

The information density matrix (Wiggins, 1972) is given by

$$|\underset{mxm}{S}| = |\underset{mxk}{U}||\underset{kxm}{U}|^t \qquad (31)$$

When S is a unit matrix, there is a perfect fit between the

observed and the predicted data. Otherwise predicted values are weighted averages of the exact data. Weighting coefficients are given by the row vectors of S. The matrix S gives a measure of the independence of the data. Usually its diagonal elements with greater magnitudes (up to a maximum of 1.0) represent the more independent observation points. For example (Aki and Richards, 1980) if

$$|S| = UU^t = \begin{vmatrix} 1 & 0 & 0 \\ 0 & .5 & -.5 \\ 0 & -.5 & .5 \end{vmatrix} \qquad (32)$$

then the prediction will fit for the first observation point but only one independent average value may be obtained over the second and third data points.

3. INVERSION OF AMPLITUDE

3.1 The Direct Problem:

The most important part of the inversion process is to develop an efficient program to solve the direct problem. Since it is particularly important to consider a model where all the model parameters contribute effectively and uniformly, the parameterization of the model under consideration demands special attention. Asymptotic Ray Theory (ART) has been used to accomodate most essential parameters in the forward problem. Zero and first order formulae (Cerveny and Ravindra, 1971) have been employed respectively for the computation of reflection and head wave amplitudes. Assuming that seismic waves travel through the elastic medium along well defined paths, the geometrical ray approach has been adopted to calculate the geometrical spreading. For simplicity we have considered an isotropic earth structure with laterally homogeneous plane multiple layers.

3.1.1 Computation of Amplitude:

Asymptotic Ray Theory (ART) provides a time domain solution to the elastodynamic equation and the boundary conditions in the form of an asymptotic ray series in inverse powers of frequency. Cerveny and Ravindra (1971) have used the ART to derive the following expressions for the vertical components of reflected and head wave amplitudes from a point source to the receiver, both located

on the surface (figure-3.1a and 3.1b).

$$L = \frac{\cos\theta_1}{v_1} \left[\sum_{j=1}^{s} (h_j v_j/\cos\theta_j)\right]^{1/2} \left[\sum_{j=1}^{s} (h_j v_j/\cos^3\theta_j)\right]^{1/2} \quad (1)$$

$$A_{refl} = \prod_{j=1}^{s} \mathcal{R}_j \eta_z/L \quad (2)$$

$$A_{head} = v_1 \tan\theta_1 \Gamma_k \prod_{\substack{j=1 \\ j\neq k}}^{s} \mathcal{R}_j \eta_z/[\omega r^{1/2}(r-r^*)^{3/2}] \quad (3)$$

k = index for the critically refracted ray segment.

L = geometrical spreading.

$\mathcal{R}_j$ = reflection or transmission coefficient corresponding to the jth ray segment.

Γ_k = head wave coefficient for critical refraction.

v_j = velocity along the jth ray segment.

h_j = thickness of the layer containing the jth ray segment.

θ_j = the angle of incidence at the jth interface on which the ray impinges.

s = total number of segments in the ray.

ω = dominant source frequency.

r = epicentral distance.

r^* = critical distance.

η_z = a unit vector tangent to the last ray segment.

To calculate multiple reflection arrivals, corresponding changes in the expression for the geometrical spreading must be made to account for the additional ray segments. The critical distance r^* is given by

$$r^* = 2 \sum_{j=1}^{n} h_j v_j (v_n^2 - v_j^2)^{-1/2} \quad (4)$$

where n is the total number of layers. Using the same

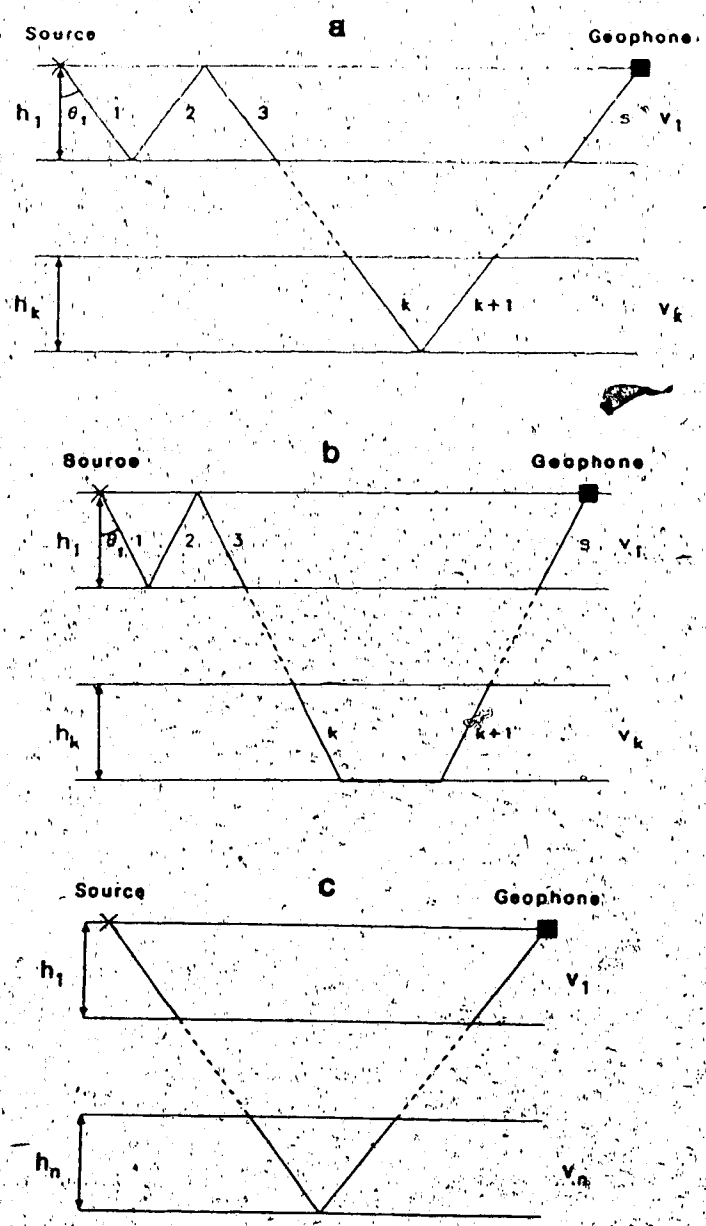

Figure 3.1 Sketch showing ray segments required to compute (a) reflection amplitudes (b) head wave amplitudes and (c) reflection travel times fo a multilayered medium.

notation as Cerveny and Ravindra (1971) the transmission coefficient R_{13}, reflection coefficient R_{11} and the head wave coefficient Γ_{131} respectively are given by,

$$R_{13} = 2\alpha_1\rho_1 P_1(\beta_2 P_2 X + \beta_1 P_4 Y)/D \tag{5}$$

$$R_{11} = -1 + 2P_1(\alpha_2\beta_2 P_2 X^2 + \beta_1\alpha_2\rho_1\rho_2 P_4 + q^2p^2 P_2 P_3 P_4)/D \tag{6}$$

$$\Gamma_{131} = 2\alpha_1\alpha_2\rho_1\rho_2\,[P_1(\beta_2 P_2 X + \beta_1 P_4 Y)^2/D^2] \text{ at } p=1/\alpha_2 \tag{7}$$

where,

$P_1 = (1 - \alpha_1^2 p^2)^{1/2}$

$P_2 = (1 - \beta_1^2 p^2)^{1/2}$

$P_3 = (1 - \alpha_2^2 p^2)^{1/2}$

$P_4 = (1 - \beta_2^2 p^2)^{1/2}$

$X = \rho_2 - qp^2$

$Y = \rho_1 + qp^2$

$Z = \rho_2 - \rho_1 - qp^2$

$q = 2(\rho_2\beta_2^2 - \rho_1\beta_1^2)$

$D = \alpha_1\alpha_2\beta_1\beta_2 p^2 Z^2 + \alpha_2\beta_2 P_1 P_2 X^2 + \alpha_1\beta_1 P_3 P_4 Y^2$
$+ \rho_1\rho_2(\alpha_2\beta_1 P_1 P_4 + \alpha_1\beta_2 P_2 P_3) + q^2p^2 P_1 P_2 P_3 P_4$

where,

$\rho_1, \alpha_1, \beta_1$ = density, P and S velocity in the layer containing the incident ray segment.

$\rho_2, \alpha_2, \beta_2$ = density, P and S velocity in the layer containing the reflected or refracted ray segment.

The ray parameter p plays an auxiliary role if the amplitude at a given epicentral distance is required. In this case p must be determined using a suitable numerical process.

3.1.2 Computation of Travel Time:

The reflection travel time at a receiver located at distance X_j is given by (figure-3.1c)

$$T_j = 2 \sum_{i=1}^{n} h_i v_i^{-1} (1 - p_j^2 v_i^2)^{-1/2} \qquad (8)$$

where n is the total number of layers. The ray parameter p_j corresponding to the offset X_j is obtained from

$$X_j = 2 \sum_{i=1}^{n} h_i p_j v_i (1 - p_j v_i^2)^{-1/2} \qquad (9)$$

using a numerical algorithm such as the Gauss-Seidel method. The head wave travel times are computed from

$$T_j = X_j / v_n + 2 \sum_{i=1}^{n} h_i (v_n^2 - v_i^2)^{1/2} \qquad (10)$$

where,

$j = 1,2,3.....n.$

n = total number of layers.

3.2 Implementation of the Method:

There are about three main considerations involved in the parameterization part of the process. The first one is the choice of dimension for the model space. Ordinary least squares suggests a small number of parameters to avoid error magnification due to ill conditioning of A^tA. Moreover it also has to be less than the dimension of the data space. Otherwise we may have to invoke a different approach (e.g.

underdetermined case) using a completely different algorithm.

The next important consideration is to try to choose parameters which are truly important variables and are expected to be resolved by the data. Of course, there are situations where the relative importance of variables is not well known beforehand. In those situations we may have to proceed with the inversion process, the variable in question being included in the parameter list and study the corresponding resolution vector. Only then we may be able to decide whether or not to discard a variable.

Lastly, the parameterization should be such that it does not lead to a complicated forward model and it is simple enough to be linearized easily and still contributes successfully towards the essential properties.

The total inversion process has been designed to work in two steps: (a) inversion of the kinematic data and (b) inversion of the dynamic data using results from the kinematic inversion as constraints. A flow diagram for the inversion scheme used in both steps (a) and (b) is shown in figure-3.2.

The kinematic inversion stage computes the P wave velocities and the layer thicknesses from the travel time data. These P velocities are then used to form part of the initial estimation required for the inversion of the dynamic information. Since a close initial guess is very important for convergence, use of this information from stage (a) significantly improves the convergence rate in stage (b). However, S wave velocities and the densities are not available from the travel time inversion in step (a). We

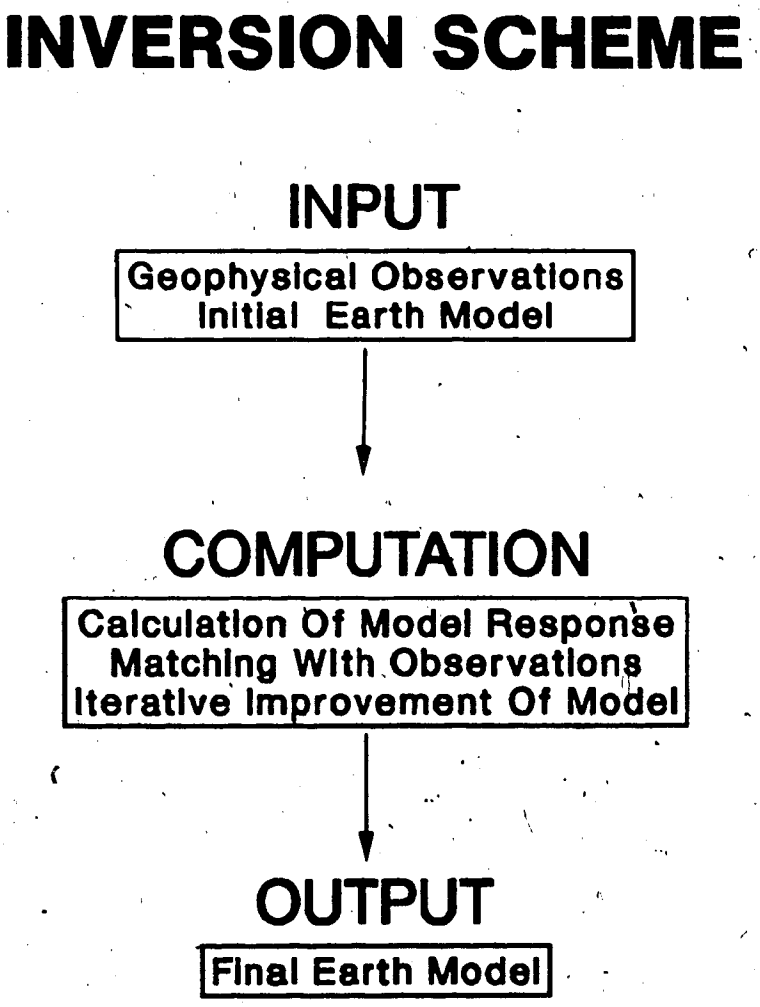

Figure 3.2 Flow diagram for the inversion scheme.

have therefore used the following formula (Birch, 1964)

$$\beta = \alpha/1.732$$
$$\rho = .252 + .3788\alpha \qquad (11)$$

to provide initial estimates of densities and S velocities which will later be refined by the inversion process. Two different approaches, (a) the stripping method and (b) the simultaneous full model inversion have been tried for the inversion scheme. In the stripping process each layer is considered separately starting from the topmost layer. Each layer has three independent parameters namely the P velocity, S velocity and density. Thickness parameters obtained from the kinematic inversion are kept constant for the rest of the inversion process. This is done intentionally to reduce the number of parameters and give more emphasis to the velocity and density values. The number of layers is indicated by the number of travel time branches in the observed seismogram. Information from the upper layers (as computed from the partial inversion) is used to reduce the number of parameters required to compute the lower layers. However, in the full model inversion all the model parameters are computed simultaneously. In the latter case, the transformation matrix A now contains information from all the specified arrivals (e.g., all first arrivals in a refraction seismogram including direct, Pg and Pn arrivals) and include the effects of all the model parameters and the data recording sites. Therefore it is obvious that the matrix dimension will be substantially larger than the previous case. Therefore, we have found the

stripping method more convenient than the full model inversion in terms of storage space, total processing time and convergence. However, the final result remains the same in both cases.

Decomposition of the matrix **A** into **U**, **Λ** and **V** has been carried out by using a subroutine given by Forsythe et al. (1977). The inversion process may be designed such that all the calculations are performed systematically without interruption and stopping at the final model automatically when the required convergence criterion is met. On the other hand, it is also possible to interrupt during calculation steps to inspect the elements of $\mathbf{A}^{-1}$ for small singular values which tend to create instability. It is also interesting to monitor results at the end of each iteration before final convergence and study the solution growth pattern. Both options ultimately lead to the same result but in most of the cases it is convenient to use the first option. Estimation of the damping parameter (equation 18, Chapter-2) may also be designed to be an automatic process (Chiu et al., 1985), but we have found that the automation process is computationally expensive and may vary for different types of data. Instead we have determined β after a few trial runs starting with a value of 1.0 and reducing it further in the subsequent steps. In most of the synthetic examples classical least squares (β=0) has been sufficient enough to omit this part of the computation.

Since ART does not produce reliable amplitudes at the critical angle, computation of the amplitudes has been restricted to the precritical or postcritical regions only. The partial derivatives which constitute the elements of the

matrix **A**, have been computed using both analytical expressions (derived in Appendix-A3) and numerical methods employing the central difference formula

$$\partial F_i/\partial X_j \simeq [F_i(X_j+\Delta X_j) - F_i(X_j-\Delta X_j]/2\Delta X_j \qquad (12)$$

Computation of response at specific geophone locations has been performed using a two-point ray tracer. The ray tracer computes the ray parameter corresponding to a specific shot-receiver pair using a numerical approach. Once the ray parameter is known the angles of incidence at each interface may be computed from Snell's law as follows

$$\theta_j = \sin^{-1}(v_j p) \qquad (13)$$

where p is the ray parameter and v_j is the velocity of the jth layer. Computation of amplitude is then straight forward using equations (1), (2) and (3).

Since the amplitude values computed by the forward model are usually very small, scaling in the form of a multiplication by a large number may be required to ensure the necessary significant digits.

3.3 Numerical Results:

Before attempting to invert real field data it is worthwhile to investigate the reliability of the inversion program developed. A series of numerical tests have been performed in this regard. The results obtained from these tests provide some insight into the capability of the

program, the consequence of inherent uncertainty in the data, error limits to the computed parameters and above all the reliability of the results produced by the program. Synthetic amplitude data (figure-3.3) have been generated by the forward model calculation of a simple 3-layer velocity model (shown as exact model in figure-3.4). Treating these amplitudes as the observation data we have used the iterative inversion algorithm to calculate the final model. As expected the final inverted model is an exact reproduction of the theoretical model (figure-3.4). Convergence to the final model occurred after 3 iterations. Absolute residues have been minimized up to the order of 10^{-5}. Table-3.1 shows the computed model parameters along with the corresponding standard deviations and resolution values. These numbers from table-3.1 imply a 100% reliable model within the specific error criteria. Overall RMS error for this inversion turns out to be 0.00002 (in terms of the differences in calculated and observed amplitudes) after just three iterations. The resolution matrix indicates a high degree of uniqueness with every diagonal element showing a maximum value of 1.0.

Next we randomly contaminated the same data with a maximum spread of 10% for the travel time data (not shown) and 5% for the amplitude data (figure-3.5). Moreover, since not all the geophones record every event we randomly deleted some of the stations to simulate this situation. It has been found that the lack of observation and contamination of the data both adversely affect the resolution and convergence rate. Moreover there is always a maximum limit of contamination (or noise) in the data which the program is

Table-3.1 Results from iterative inversion of exact amplitude data for a 3-layer model.

Layer	Exact model	Inverted Model	Resolution (diagonal)	Standard Deviation
	P-Velocity km/s			
1	6.0	6.000	1.00	.00001
2	6.5	6.500	1.00	.00001
3	7.0	7.000	1.00	.00002
	S-Velocity km/s			
1	3.464	3.464	1.00	.00001
2	3.753	3.753	1.00	.00002
3	4.042	4.042	1.00	.00002
	Density gm/cc			
1	2.525	2.525	1.00	.00001
2	2.714	2.714	1.00	.00003
3	2.904	2.904	1.00	.00003

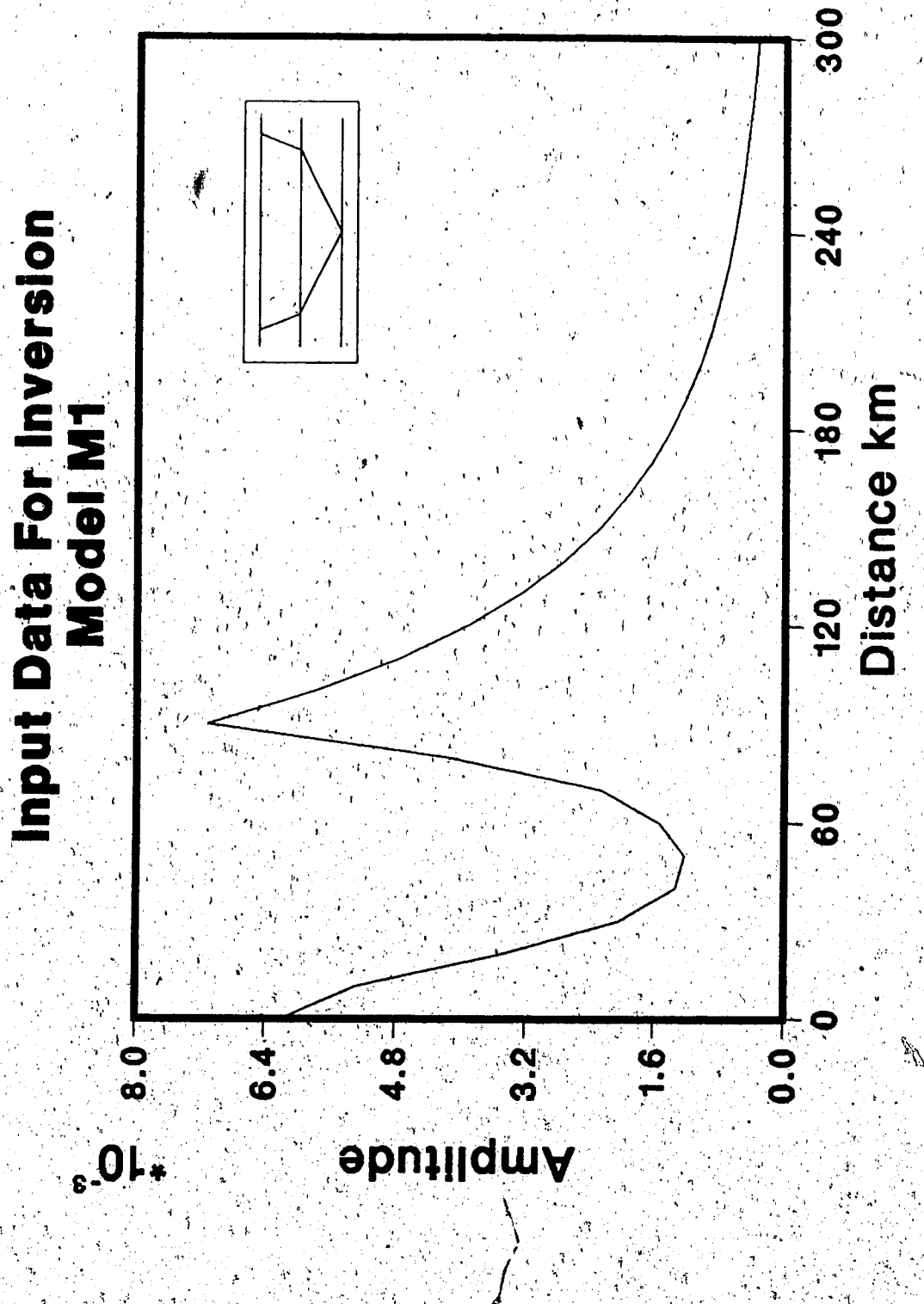

Figure 3.3 Noise free synthetic amplitude data obtained from forward calculation of model M1 shown in figure-3.4.

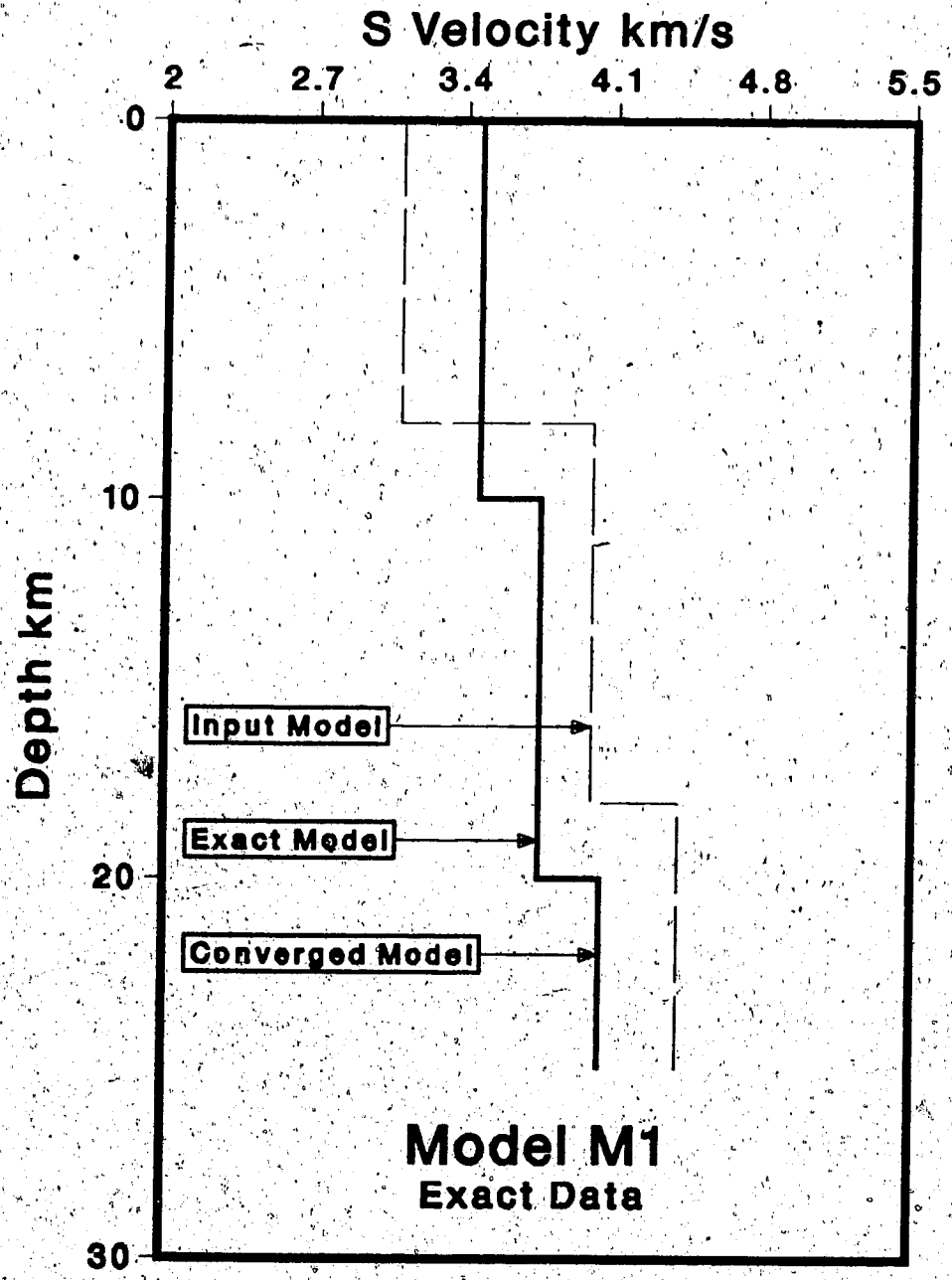

Figure 3.4 Inverted velocity model M1 from noise free amplitude data shown in figure-3.3.

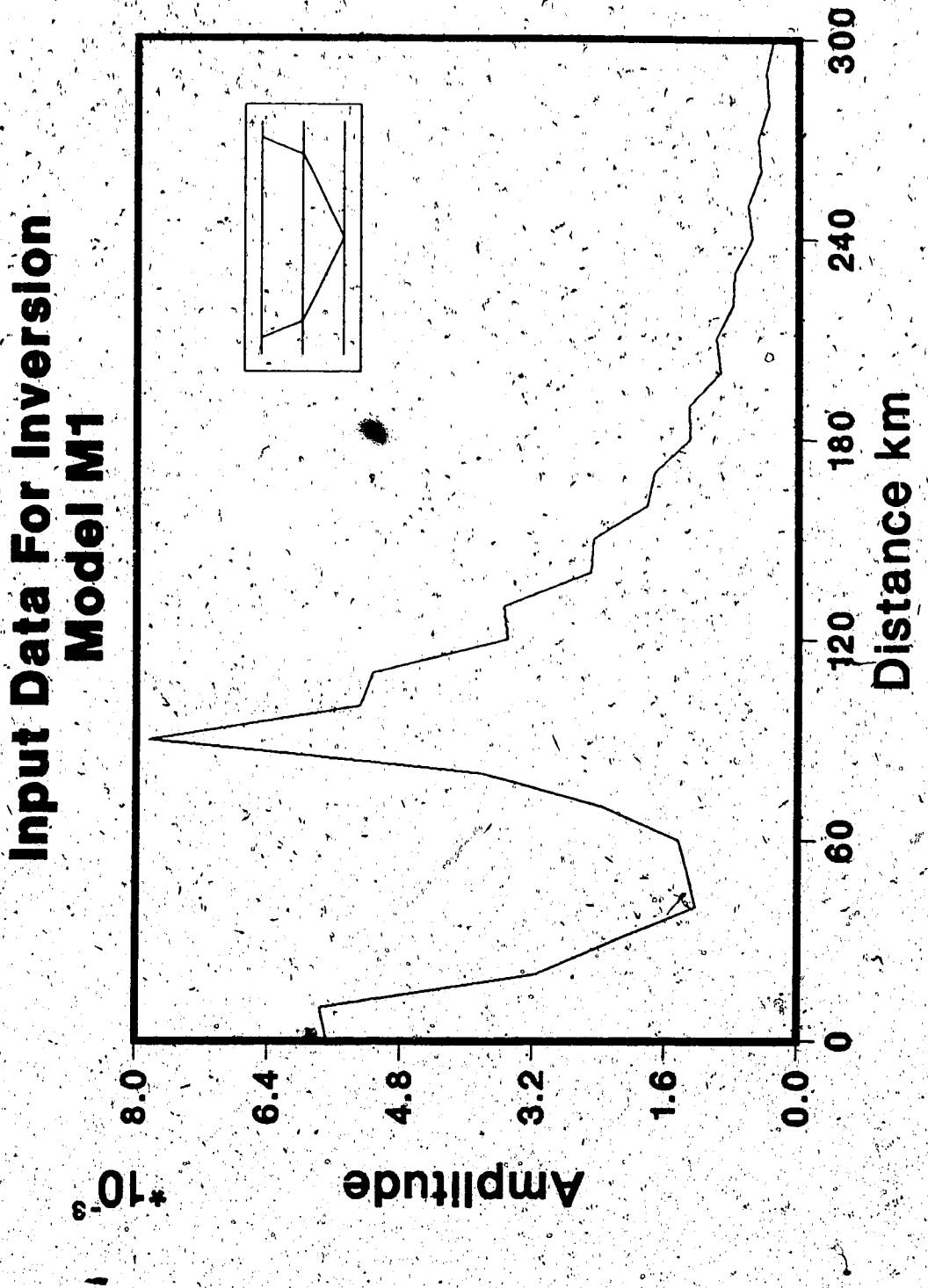

Figure 3.5 Noisy synthetic amplitude data for model M1.

able to tolerate while still producing a model reasonably close to the exact one. We have found that a maximum of 10% contamination to the data is allowable to get an acceptable estimate of the solution, provided the initial model is a close guess to the actual model. The results from the inversion of contaminated data are included in table-3.2 and the final model is shown in figure-3.6. The noise RMS of amplitudes remaining after 5 iterations is 0.01. It is also evident that the parameters for the inverted model now show larger standard deviations than those obtained with exact data. However, if the estimated model parameters are judged along with the estimated deviations, the agreement is still good. Therefore we may conclude that the program will work for both exact and noisy (within the above limits) data by carefully detecting the noise level (absolute residues left at the end of inversion), giving a quantitative estimate of the uncertainty (standard deviation) of the computed values and indicating the reliability (resolution) of the results.

We have also tried different starting models and found that while the final solution usually does not depend on the initial model, the convergence rate generally does, as would be expected.

The next example we have attempted is the noisy amplitude data (figure-3.7) generated from a 3-layer model with a low velocity zone in the middle crust. From the results of the inversion (shown in table-3.3 and figure-3.8) it is clear that the program has no difficulty in detecting such anomalies in the model.

Another example we have considered is the multiple reflection arrivals from the second layer in a three layer

Table-3.2 Results from iterative inversion of contaminated amplitude data for a 3-layer model.

Layer	Exact model	Inverted Model	Resolution (diagonal)	Standard Deviation
	P-Velocity km/s			
1	6.0	6.036	1.00	.04631
2	6.5	6.550	1.00	.05752
3	7.0	7.045	1.00	.05241
	S-Velocity km/s			
1	3.464	3.500	1.00	.05250
2	3.753	3.807	1.00	.06120
3	4.042	3.993	1.00	.05701
	Density gm/cc			
1	2.525	2.531	1.00	.03190
2	2.714	2.742	1.00	.02912
3	2.904	2.856	1.00	.04232

Table-3.3 Results from iterative inversion of amplitude data for a 3-layer low velocity model.

Layer	Exact model	Inverted Model	Resolution (diagonal)	Standard Deviation
	P-Velocity km/s			
1	6.5	6.458	1.00	.06640
2	6.0	5.963	1.00	.04755
3	7.0	6.941	1.00	.07160
	S-Velocity km/s			
1	3.753	3.700	1.00	.05139
2	3.464	3.420	1.00	.06252
3	4.042	3.950	1.00	.09170
	Density gm/cc			
1	2.714	2.679	1.00	.04142
2	2.525	2.496	1.00	.05350
3	2.904	2.944	1.00	.08366

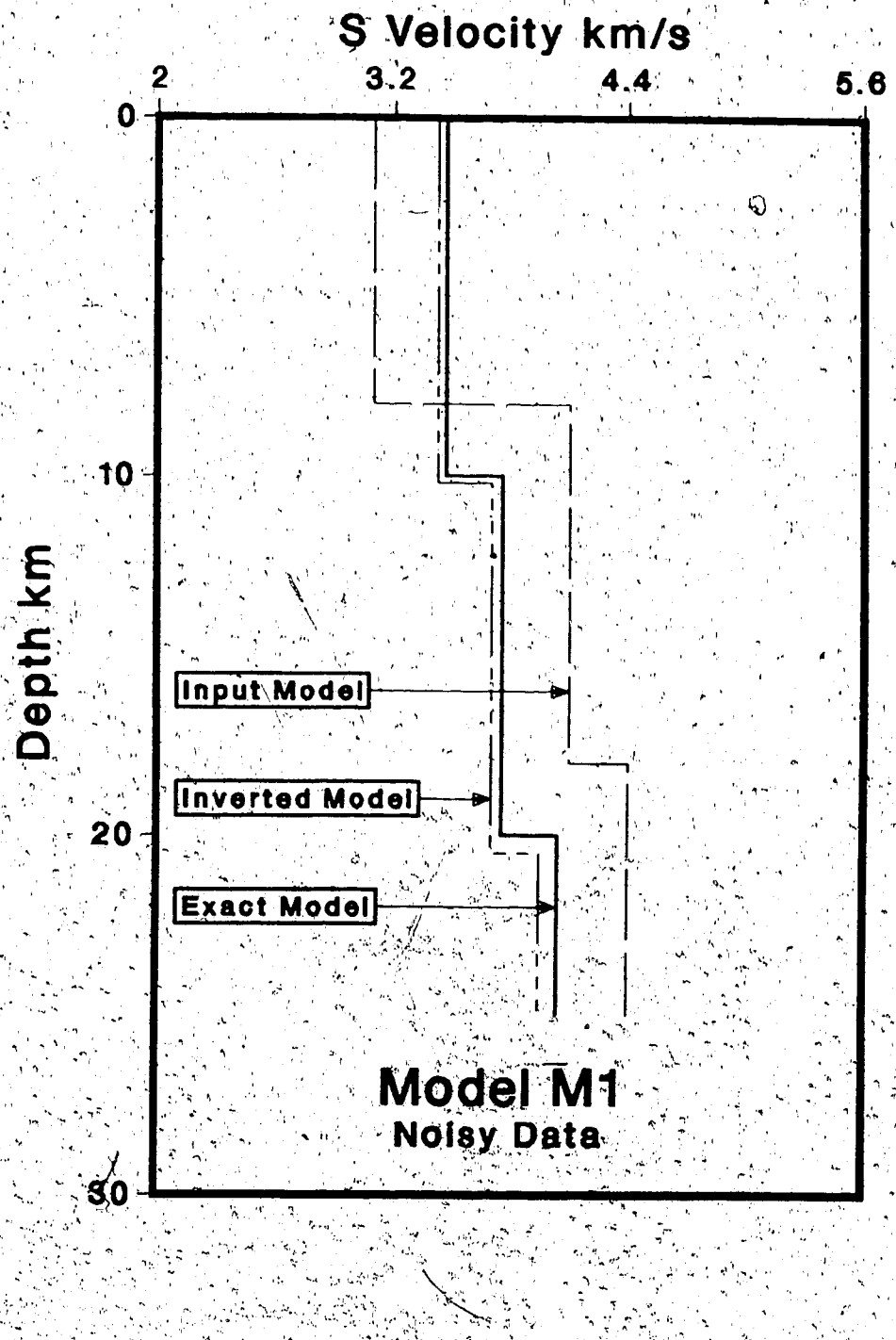

Figure 3.6 Inverted shear wave velocity model M1 obtained from the noisy amplitude data shown in figure-3.5.

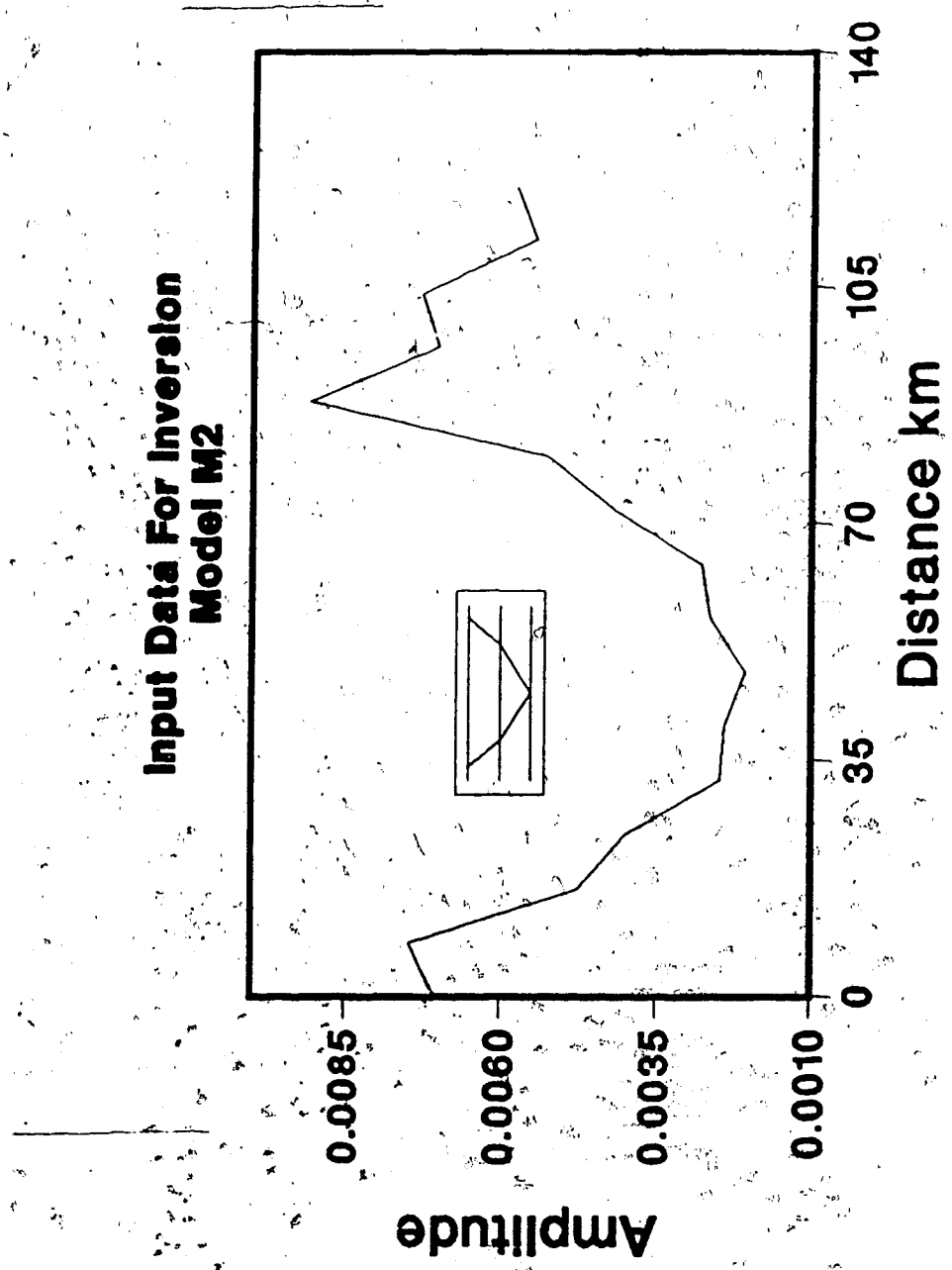

Figure 3.7 Synthetic amplitude data for a 3-layer model M2 with a low velocity zone in the middle crust.

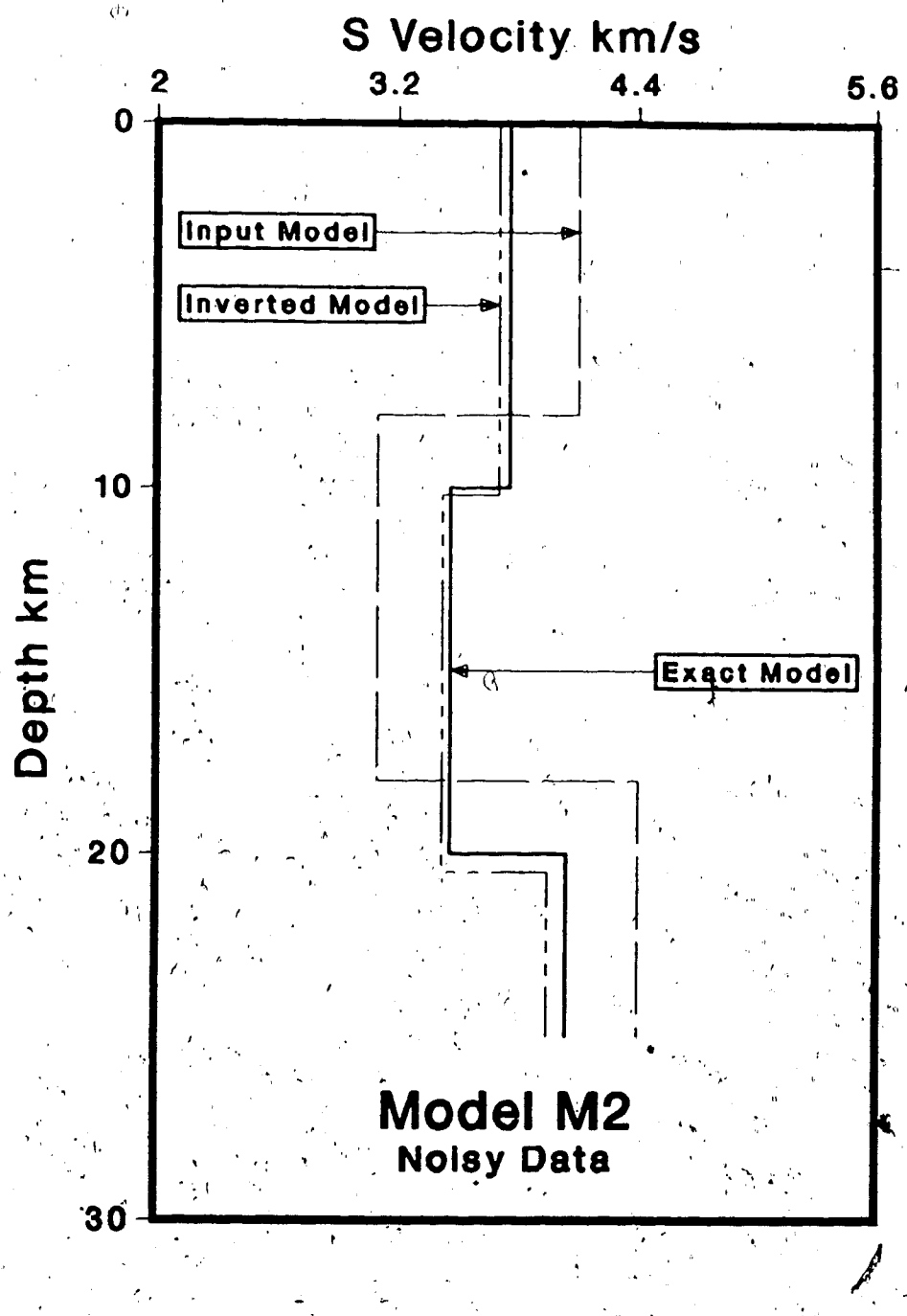

Figure 3.8 Results of inversion of noisy amplitude data shown in figure-3.7 for the low velocity model M2.

model (the program works for multiples from any interface of a layered model). From visual inspection of the field seismogram alone it is particularly troublesome to decide whether a primary or a multiple reflection arrival is being observed. Sometimes these multiples may be attenuated during the Common Depth Point (CDP) processing but unfortunately the Normal Move Out (NMO) is not usually large enough to identify the multiples with certainty. For long range profiles such as in the case of wide angle data it is particularly difficult to detect such arrivals. An effective diagnostic clue to the identification of multiples would be to consider the energy of the signals but merely visual inspection would not suffice due to the presence of noise in the record. Therefore we suggest the application of our inversion algorithm as an attempt to resolve this problem. Even if the visual identification may seem extremely difficult we may try different input models until it is established that no other solutions are possible except the one with multiple arrivals. A trial and error process may be required but a solution based on the primary arrival assumption is most unlikely to occur. This is because of the sensitivity of the amplitude function in terms of depth, reflectivity and geometrical divergence of the wave front. Figure-3.9 shows the test data we have considered. Figure-3.10 and table-3.4 include all the results obtained from the iterative inversion of contaminated multiple reflection arrivals. Table-3.5 shows the result of an attempt to invert a set of noise free multiple reflection data in terms of an intentional wrong assumption of primary arrivals. The program unsuccessfully

Table-3.4 Results from iterative inversion of noisy multiple reflection amplitude data.

Layer	Exact model	Inverted Model	Resolution (diagonal)	Standard Deviation
	P-Velocity km/s			
1	6.0	6.036	1.00	.0323
2	6.5	6.550	1.00	.0510
3	7.0	7.045	1.00	.0432
	S-Velocity km/s			
1	3.464	3.500	1.00	.0457
2	3.753	3.807	1.00	.0561
3	4.042	3.993	1.00	.0282
	Density gm/cc			
1	2.525	2.531	1.00	.0234
2	2.714	2.742	1.00	.0346
3	2.904	2.856	1.00	.0584

Table-3.5 Results from iterative inversion of multiple reflection data with wrong primary arrival assumption.

Layer	Exact model	Inverted Model	Resolution (diag.)	Standard Deviation
	P-Velocity km/s			
1	6.0	7.206	1.00	1.8500
2	6.5	8.495	1.00	2.1200
3	7.0	9.045	1.00	2.0130
	S-Velocity km/s			
1	3.464	4.371	1.00	1.5700
2	3.753	4.950	1.00	1.8640
3	4.042	5.885	1.00	1.8660
	Density gm/cc			
1	2.525	2.202	1.00	.43030
2	2.714	2.316	1.00	.54310
3	2.904	3.612	1.00	.67420

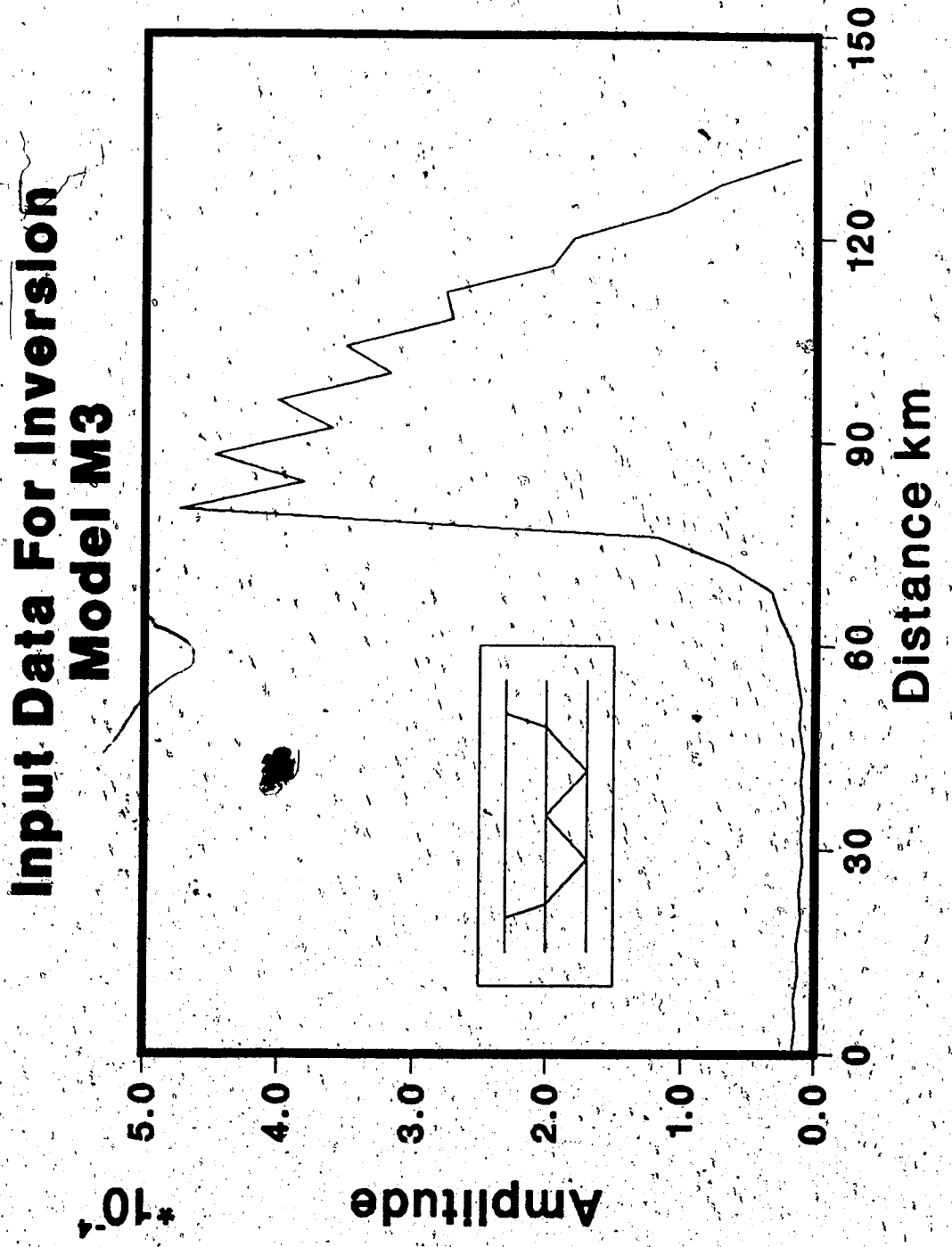

Figure 3.9 Synthetic amplitude data for the velocity model M3 containing multiple reflection arrivals.

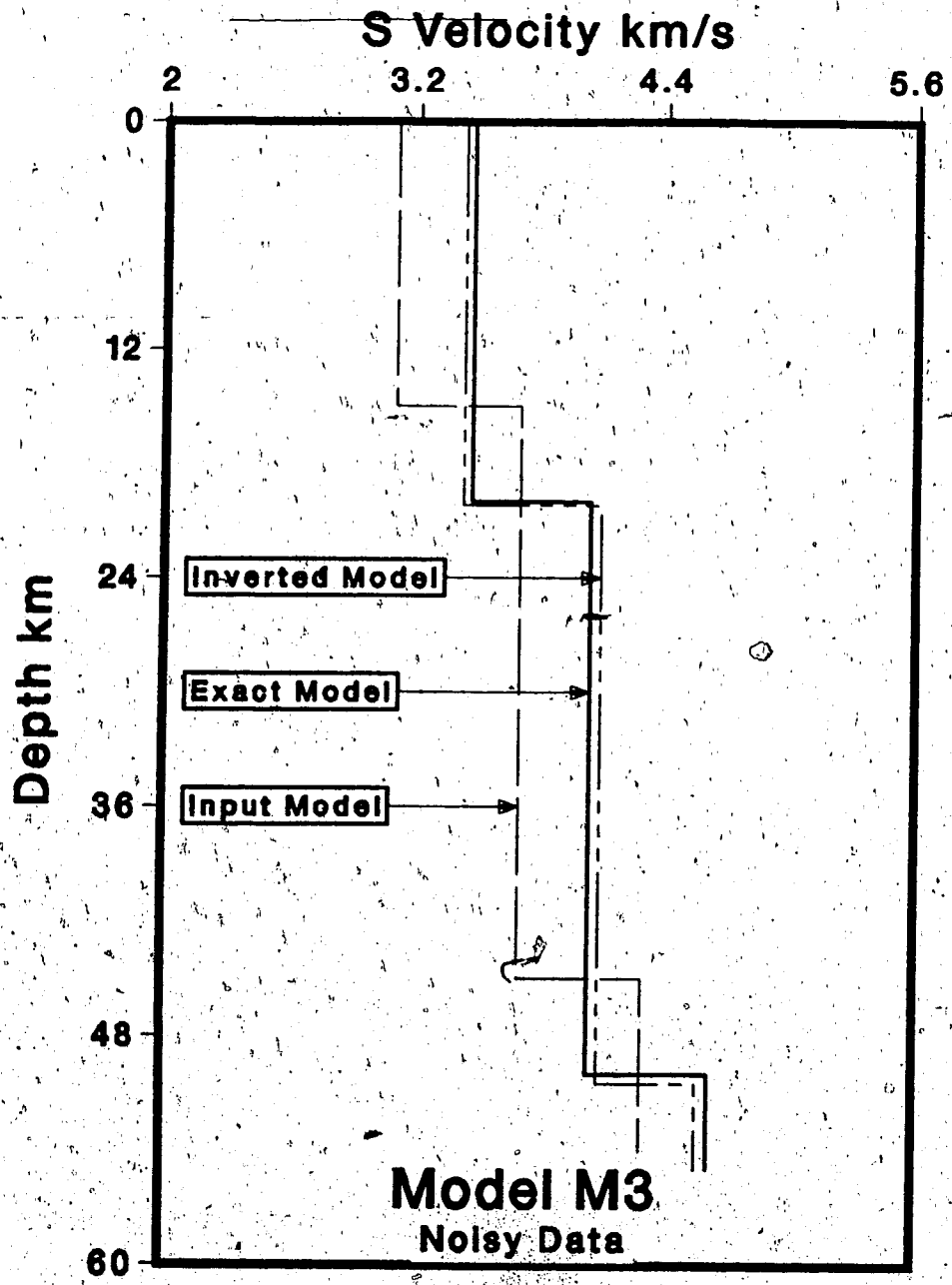

Figure 3.10 Inverted velocity model M3 from noisy multiple reflection amplitude data shown in figure-3.9.

attempts to find a local minimum around the approximate initial solution. As expected the result is an absolute non-convergence. Even after 200 iterations the program fails to converge to a realistic model. Another test for inversion attempt with primary arrival data in terms of wrong multiple arrival assumption also led to divergence. Similar results from several other tests with different models encouraged us to assume that the program is useful in detecting multiples in many difficult situations by indicating a probable wrong assumption about the phase under consideration in which case the inversion attempt usually leads to a divergence.

4. CRUSTAL MODELS WITH CURVED BOUNDARIES

Deformed crustal regions and also many sedimentary basins often demand modeling in terms of curved structures. Two dimensional geosynclines or anticlinal surfaces are adequately described if the centre and radius of curvatures are known. Forward analytical models in terms of parameters such as P wave velocity, radius and centre of curvatures are considered to determine these quantities from observed wide-angle reflection travel times. Synthetic models using convex and concave shaped interfaces and also extended curved surfaces having both convex and concave type undulations are used to demonstrate that the linearized inverse method can be used efficiently to determine the curved nature of the reflecting boundaries. Analytical computation of the forward model is used to ensure rapid convergence and nominal computer cost. It is interesting to note that since radius of curvature is calculated as an output from the travel time inversion the Asymptotic Ray Theory may be used to calculate the amplitudes from analytical expressions given by Cerveny and Ravindra (1971) virtually for no additional cost. This information may also be used to generate synthetic seismograms for curved structures with small computer cost. Further inversion of the observed amplitudes will resolve additional unknowns such as density and S wave velocities of both top and bottom side of the reflector. Homogeneous two layer models are considered throughout for simplicity. More complex structures may be used with appropriate ray tracing in the forward model.

4.1 Forward Model:

Expression for travel times of reflected body waves from a curved surface in parametric form is given by (Meshbei, 1968)

$$T = \frac{(x^2+z^2)^{1/2}}{v_1}\left[1 + \frac{za}{b-c}\right] \qquad (1)$$

$$D = (x+zd)\left[1 + \frac{za}{b-c}\right] \qquad (2)$$

where D is the offset distance. It is assumed that the recording profile is perpendicular to the strike of the structure. The following terms have been used in equations (1) and (2) above

v_1 = velocity of homogeneous medium above the reflector

$a = 1 + d^2$

$d = \frac{\partial z}{\partial x} = \pm\frac{x-x_0}{\sqrt{[r_0^2-(x-x_0)]}}$

d = ± means a concave and a convex surface respectively

$z = z_0 \pm [r_0^2-(x-x_0)^2]^{1/2}$

x_0 = x-coordinate of centre of curvature

z_0 = z-coordinate of centre of curvature

r_0 = radius of curvature

$b^2 = (x^2+z^2)a - (x+zd)^2$

$c = (x+zd)d$

x, z = coordinate for the reflection point.

It is important to note that equations (1) and (2) remain valid for various types of ideal curvatures such as circular, elliptical and parabolic interfaces. However, for each type of surface an appropriate value for the tangent d to the curved boundary at the reflection point has to be found either analytically or numerically. Approximate

initial values for x_0, r_0, z_0 and the known offset distance D are inserted into equation (2) to solve for the x coordinate of the reflection point by an iterative method. Thus found, the x coordinate forms an estimate corresponding to the current values of x_0, r_0 and z_0. The inversion process is then carried out in terms of x_0, r_0, z_0, and v_1 using equation (1) as the expression for the response function. Iterations proceed until convergence is met using a suitable tolerance criterion (see equation (15), chapter-2).

4.2 Synthetic Tests:

4.2.1 Convex Surface:

Geometrical rays are considered to be reflected from a convex boundary of continental scale (figure-4.1). Synthetic data generated from this model (Model 2CM1) are shown in figure-4.2. Application of the inversion program to this data set results in an exact reproduction of the theoretical model within three iterations (table-4.1). Travel time residues were minimized up to 0.0001 sec. Repeated modeling with contaminated data reveals that the problem is highly non-linear and ill-conditioned. This is indicated by an increased number of iterations for convergence and large variations in the final results with only small changes in the input parameters. Therefore to avoid severe non-linearity and ill conditioning scaling of the transformation matrix A (Chapter-2) was used with only a 5% contamination to the data set. Application of a damped least squares method in addition, gave the required

Table-4.1 Results after inversion of synthetic reflection travel times shown in figure-4.2 in terms of a convex shaped interface model 2CM1.

	Xo (km)	Zo (km)	Ro (km)	V (km/s)
Exact model	10.00	20.00	10.00	6.400
Initial Model	11.00	22.00	11.00	6.900
Inverted Model	10.00	20.00	10.01	6.400
Resolution	1.000	1.000	1.000	1.000
Standard Deviation	.0002	.0010	.0014	.0001

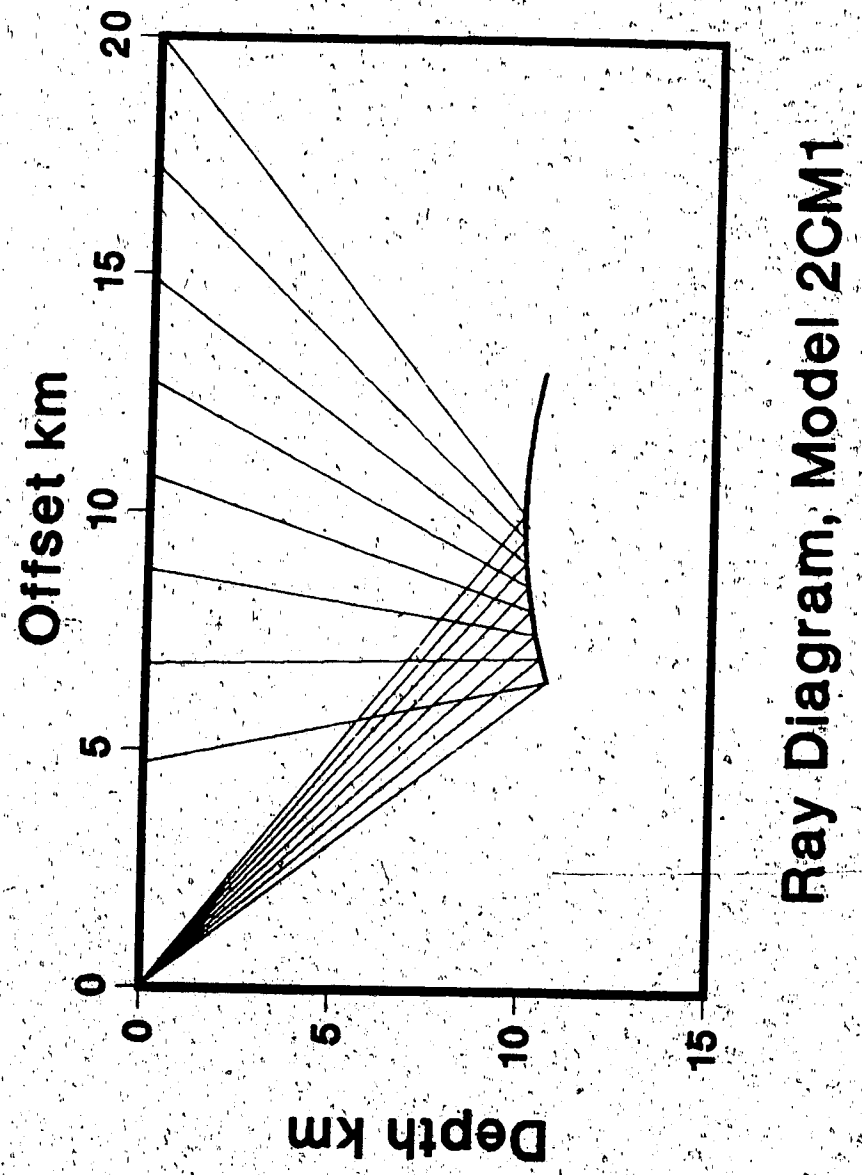

Figure 4.1 Model 2CM1: Test model of a 2-layer convex shaped crustal reflector boundary.

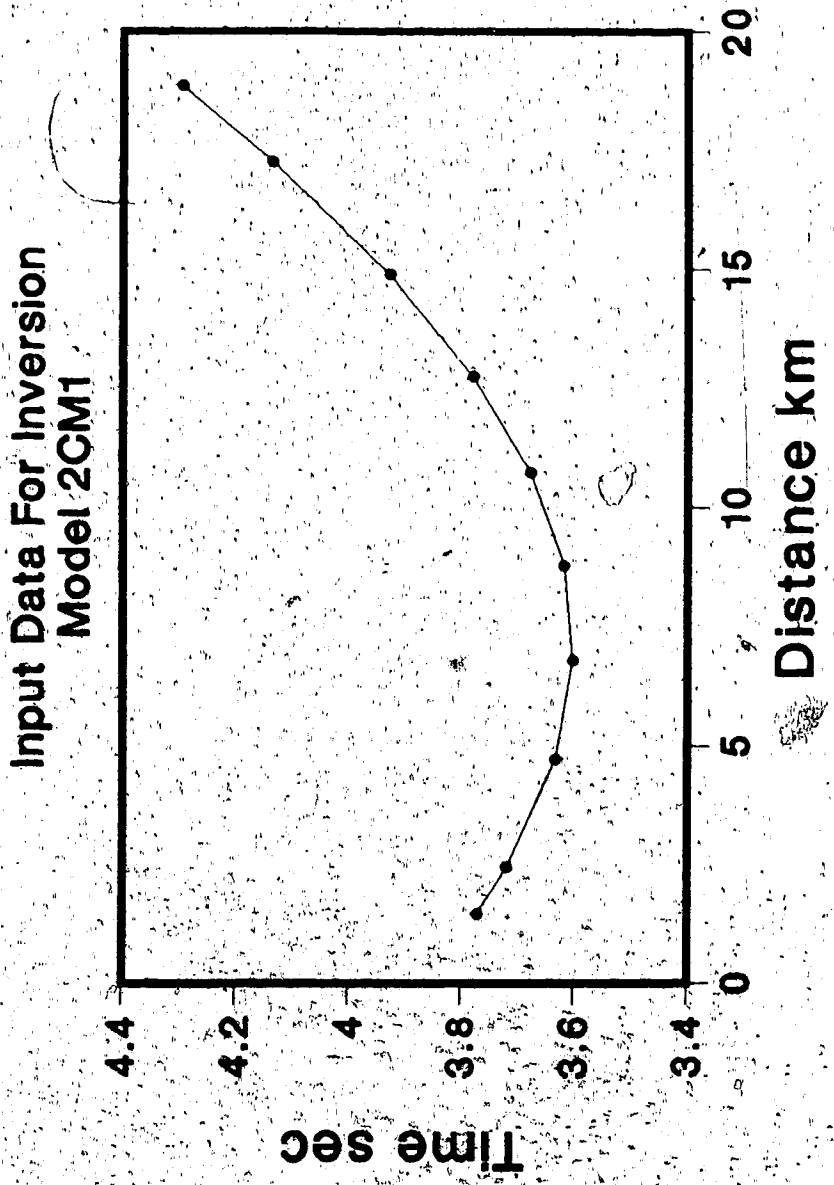

Figure 4.2 Travel time data generated from a convex shaped crustal reflector shown in figure-4.1.

stability.

4.2.2 Concave Surface:

Similar modeling with artificial concave structures were performed using the damped least squares technique. The data (figure-4.3) obtained from the forward model calculation of the known structure (Model 2CM2, figure-4.3) were inverted after adding random noise. Convergence was achieved after 6 iterations. A close initial guess was necessary to achieve convergence. Table-4.2 shows the results of inversion. Absolute residues were reduced up to 0.001 sec.

4.2.3 Extended Curved Interface:

Application of the iterative inversion algorithm to extended curved interfaces may be possible using the concepts used earlier in the case of convex or concave interfaces. The entire section of the data set may be divided into several hypothetical subsections each of which corresponds to a single unit of the total extended boundary. It is difficult to establish beforehand, whether a convex or concave unit is being treated. It has to be decided by a trial and error process. Sometimes an experienced geophysicist may recognize the nature of the curvature by looking at the travel time curve alone. The division of the curved boundary into smaller units is regulated by the requirement that each unit must correspond to a minimum number of data points so that a least squares criterion may

Table-4.2 Results after inversion of synthetic reflection travel times shown in figure-4.4 in terms of a concave shaped interface model 2CM2.

	Xo (km)	Zo (km)	Ro (km)	V (km/s)
Exact model	20.00	20.00	20.00	6.400
Initial Model	22.00	22.00	22.00	6.900
Inverted Model	20.01	20.01	20.01	6.400
Resolution	0.956	0.833	0.588	0.999
Standard Deviation	.0040	.0052	.0069	.0002

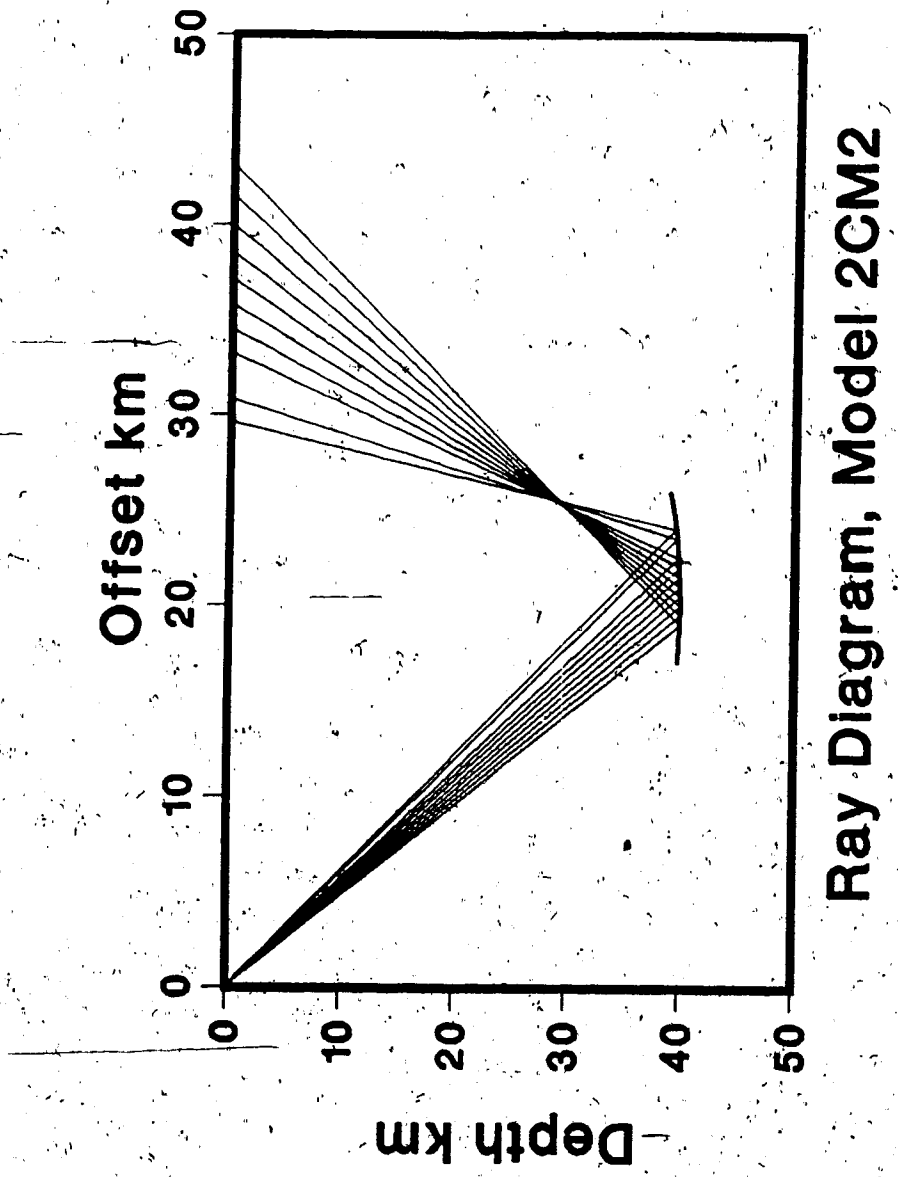

Figure 4.3 Model 2CM2: Test model used to calculate travel time data shown in figure-4.4.

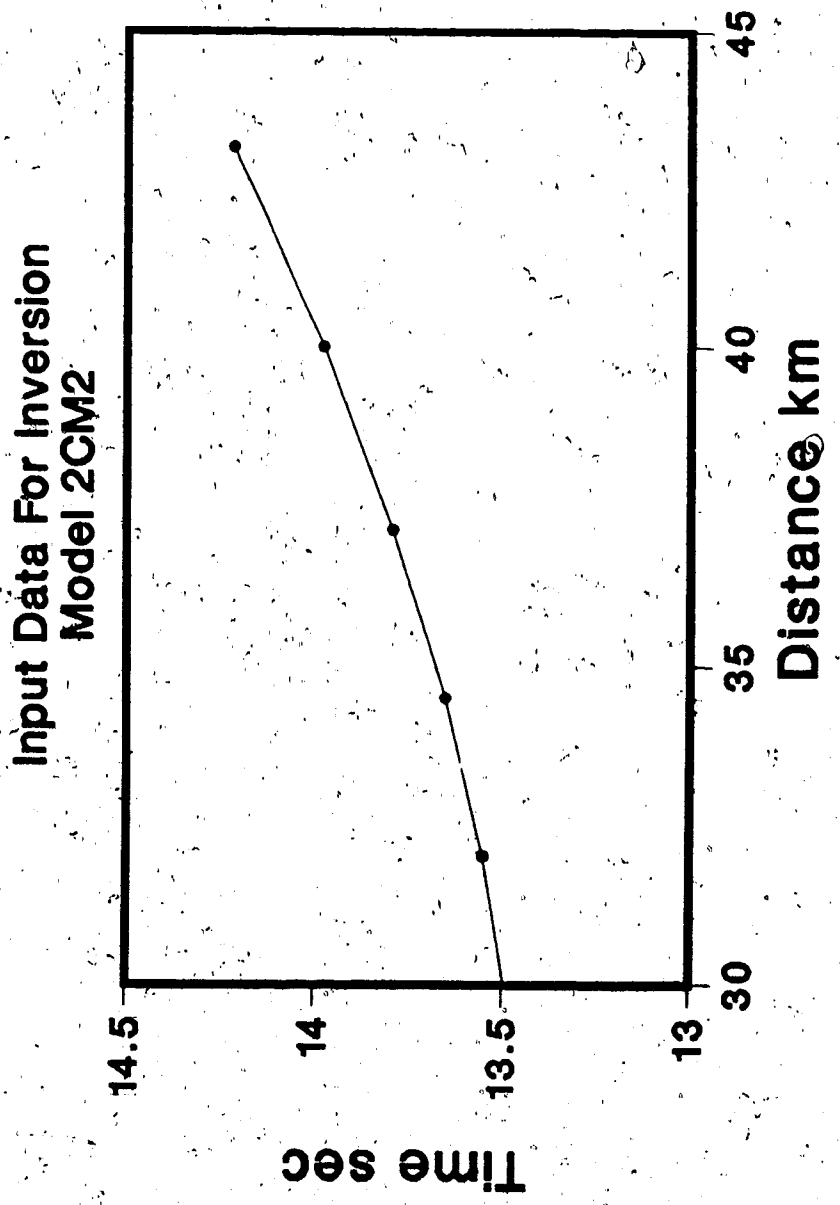

Figure 4.4 Travel time data for theoretical model 2CM2 shown in figure-4.3.

be applied. Figure-4.6 shows the data points used to determine the extended curved boundary (Model 2CM3, figure-4.5) from the curvatures of its three sub units. Two convex surfaces and a concave interface form a composite sinusoidal type extended boundary. The results of inversion are listed in table-4.3. It is obvious that the assumption of smaller curved sections demands a large number of model parameters. For better mapping of the curved boundary it is also necessary to consider as many reflecting points as possible on the interface. Therefore, it is of advantage to have densely situated recording sites. Figure-4.7 is presented as an example to show that realistic structures may not be resolved well with only a single shot point. Due to random orientation of the curved sections many of the reflected rays register on the surface at regions well beyond the observation area. Therefore multiple shot points are suggested whenever possible.

The results of the inversion indicate that it is possible to invert successfully the reflection arrivals from general curved structures of 2-D nature. Results may be improved with more shot points and closely spaced observation points. Once again the limit of the random contamination that may be handled safely is only 5% due to severe non-linearity and ill conditioning.

4.2.4 Field Examples:

The field data have been taken from a refraction seismogram recorded by the COCRUST group in 1979 along a south-north profile in central Saskatchewan (figure-4.8).

Table-4.3 Results after inversion of synthetic reflection travel times shown in figure-4.6 in terms of an extended curved interface model 2CM3. X1,Z1 and R1 = coordinate of centre curvature and radius of curvature for first interface unit etc.

km or km/s	Exact Model	Inverted Model	Resolution	Standard Deviation
V1	6.40	6.400	1.00	0.0058
X1	20.0	20.01	1.00	0.0121
Z1	50.0	50.02	1.00	0.0279
R1	20.0	20.03	1.00	0.0156
X2	60.0	59.98	.978	0.0091
Z2	30.0	29.97	.919	0.0175
R2	20.0	20.06	.575	0.0499
X3	100.0	100.30	1.00	0.2067
Z3	50.0	50.56	1.00	0.4307
R3	20.0	20.67	1.00	0.5387

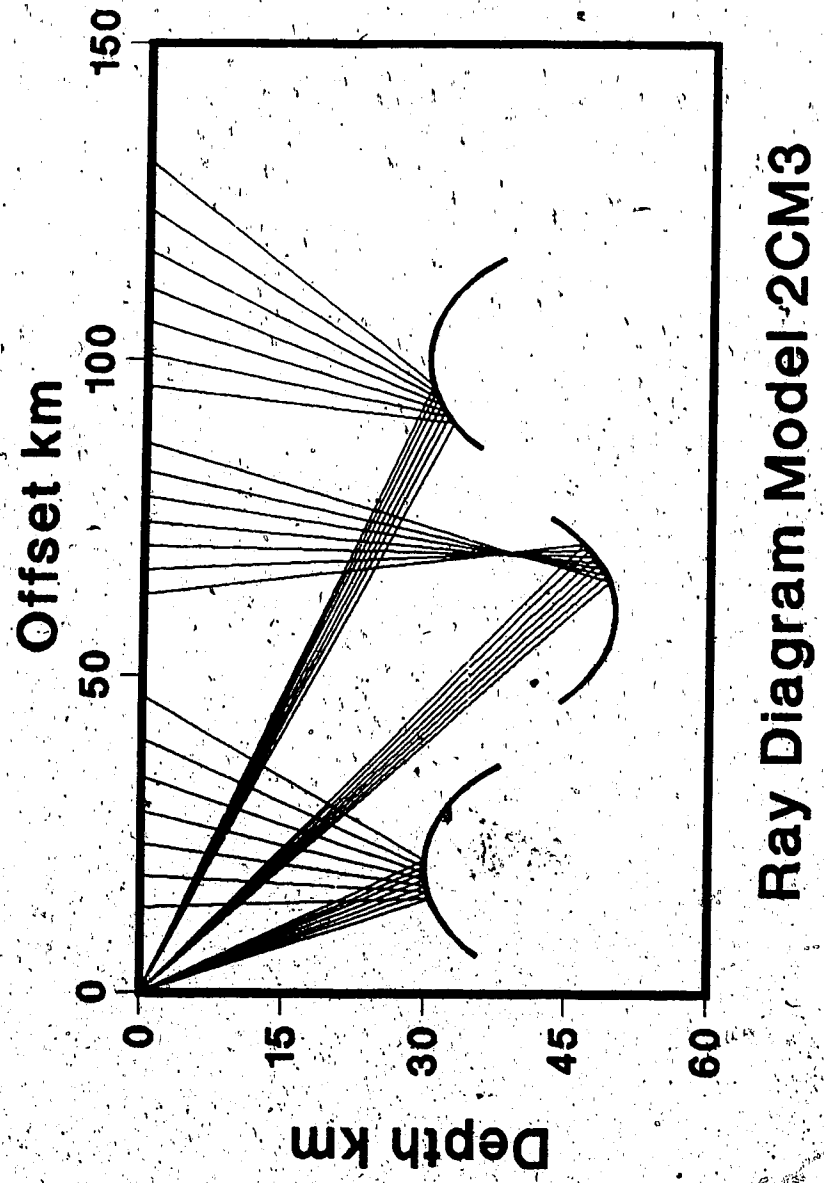

Figure 4.5 Model 2CM3: Test model for an extended curved reflector.

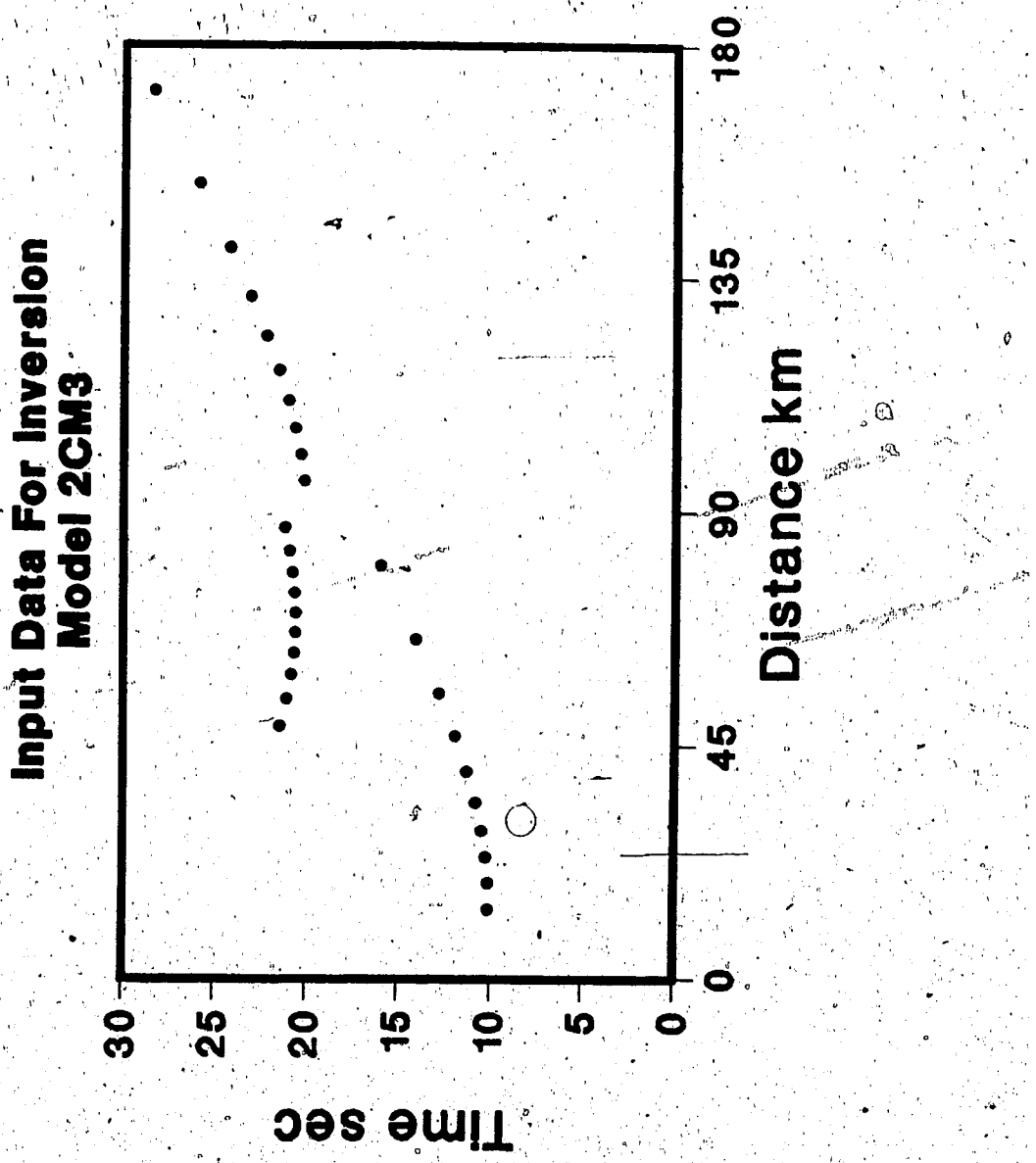

Figure 4.6 Travel time data generated artificially from a 2-layer test model of extended reflector shown in figure-4.5.

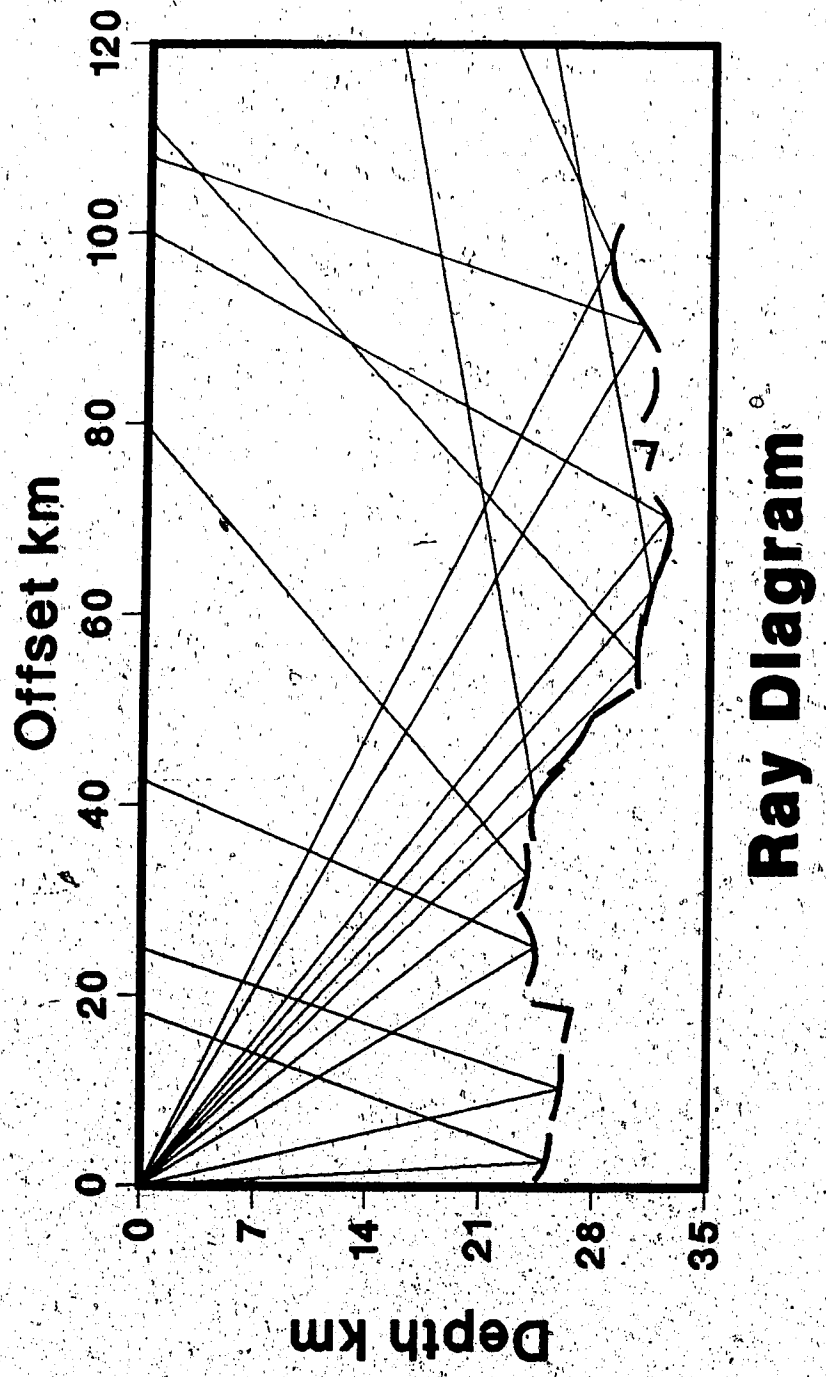

Figure 4.7 Alberta Model: Reflector approximated as a composite of smaller curvature units (modified from Hron et al., 1977).

The PmP arrivals used in the inversion process have been marked with asterisks. Results of the inversion (table-4.4) in terms of a curved reflector show that the Moho surface under study does not have marked undulations. A flat interface is suggested by a large radius of curvature. This result is supported by the interpretation of the first arrival travel time data by Hajnál et al. (1984). In the next chapter modeling of these observations in terms of 2-D dipping boundaries will again confirm the flat nature of the Moho surface in this area. The average velocity of the upper medium is 6.4 km/s. Depth of the reflector called the Moho is found to be 46.7 kms. The Root Mean Square (RMS) value of the noise was reduced as much as 0.3 sec. This value is somewhat higher than the usual travel time picking error of 0.1 sec. As a result large values of standard deviations have been calculated for the model parameters. In chapter-5 it has been shown that the RMS value of the noise may be reduced as much as 0.1 sec which suggests that these data are better represented by a 2-D arbitrarily dipping model. Inversion attempts to model the present data set in terms of curved boundaries indicate that the curved model does not fit the data closely and an output result with large radius of curvature clearly shows that the structure does not have any wave-like attitude.

Table-4.4 Results of inversion of field travel time data (COCRUST line B S-N, 1979) shown in figure-4.8 in terms of a curved reflector model.

	Xo (km)	Zo (km)	Ro (km)	V (km/s)
Initial Model	100.00	445.00	400.00	6.90
Inverted Model	95.02	481.50	434.80	6.51
Resolution	1.00	.987	.986	1.00
Standard Deviation	1.48	34.4	36.4	.049

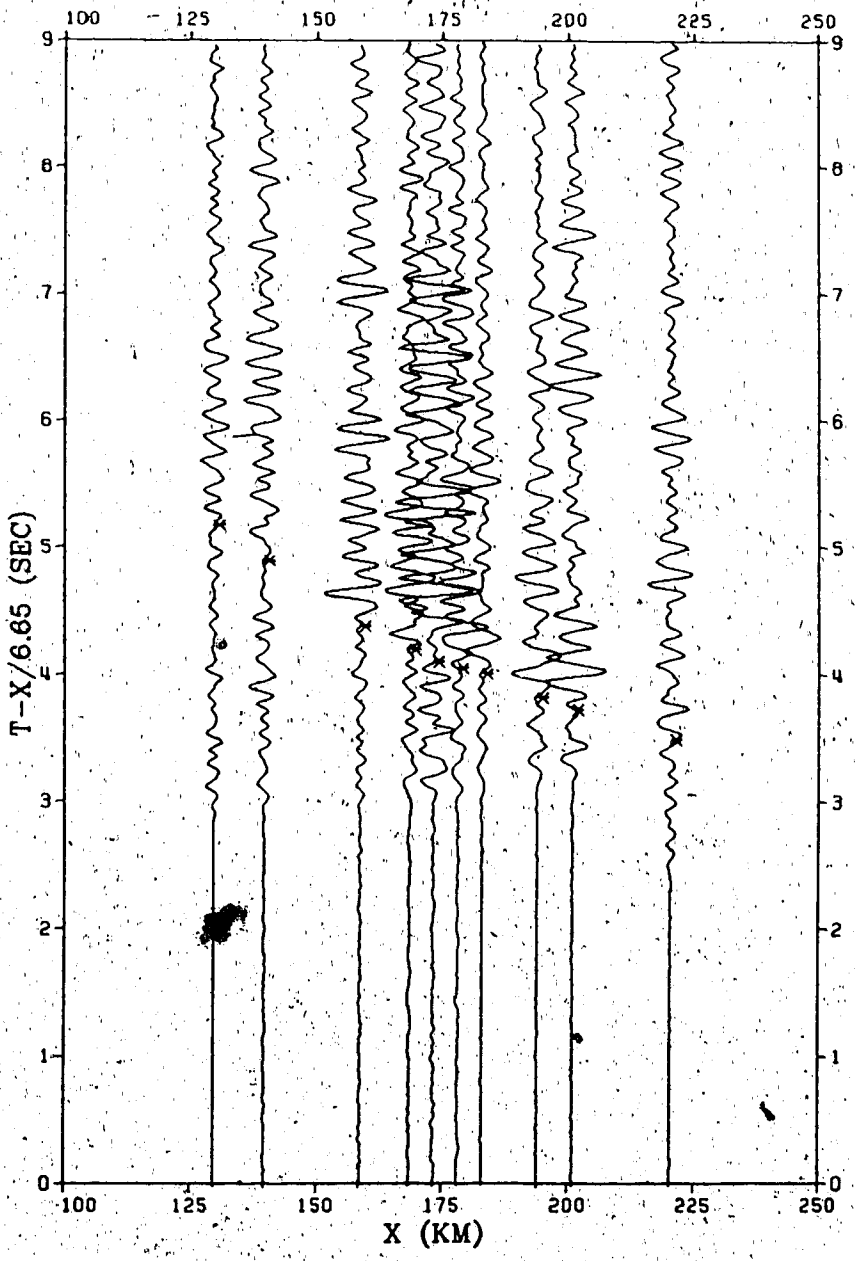

Figure 4.8 Travel time data indicating PmP arrivals by asterics in the wide angle seismogram recorded by COCRUST group along a south-north profile in central Saskatchewan.

5. CRUSTAL MODELS WITH 2-D DIPPING BOUNDARIES

Realistic approximation to many geological structures may be achieved by adopting a forward model in terms of 2-D plane interfaces of arbitrary dips. It is easy to construct geometrical rays if the medium is homogeneous and the reflecting interface is allowed to change its dip direction arbitrarily. However a few assumptions are necessary to make the calculations valid. First we have to assume that the reflection points are confined to the planar parts of the interface. This will allow us to ignore scattered and diffracted rays from the corner points where the interface changes its dip direction. Secondly we assume a simple two-layer medium. Thirdly we ignore the refracted rays for simplicity.

5.1 Forward Model:

Total travel time for a ray reflected from a dipping interface located at depth Z below the shot point with source and receiver both located on the surface is given by (Dobrin, 1976)

$$T = \frac{2Z}{V}\left[1 + \frac{D^2}{4Z^2} + \frac{D}{Z}\sin\alpha\right]^{1/2} \qquad (1)$$

where,

V = velocity of the upper medium.

Z = perpendicular to reflector depth below the shot point.

D = offset distance.

α = dip angle of the boundary in degrees.

It is assumed that the reflecting boundary is composed of several sub units each corresponding to a group of observations having a minimum of three data points in it. Each group when inverted through the iterative process will generate one single dipping interface unit. The parameters computed for each group are V, D and α. Coordinates of the reflection points are determined by solving two simultaneous equations obtained from the known path length of the ray and the Snell's law for equality of incident and reflecting angles in the homogeneous medium (Appendix-A7).

5.2 Synthetic Examples:

M2D1 shown in figure-5.1 is a two-layer synthetic model having the reflecting boundary as a composite of three sub-interfaces of different dips. Three groups of geophones record the arrivals reflected from these three sub interfaces. Synthetic data (figure-5.2) are generated using the forward model calculation of equation (1). The inversion is carried out for these observations to obtain the results listed in table-5.1. The vertical depths of sub interfaces below the source point along with the corresponding dips are converted to the coordinates of the reflection points (table-5.2) using equations given in Appendix-A7.

Next we consider another synthetic example (Model M2D2, figure-5.3) involving large dip angles similar to those observed in the subduction zones. Artificial data obtained using equation (1) for this model are shown in figure-5.4.

Table-5.1 Results from iterative inversion of wide angle reflection travel times in terms of of arbitrarily dipping interface model M2D1.

	Velocity (km/s)	Depth (km)	Dip Angle (deg)
INTERFACE UNIT # 1			
Initial	6.500	11.000	15.000
Final	6.399	9.997	13.997
Resolution	1.000	1.000	1.000
Standard Deviation	0.001	0.003	0.003
INTERFACE UNIT # 2			
Initial	6.500	22.000	0.002
Final	6.403	19.947	0.133
Resolution	1.000	1.000	1.000
Standard Deviation	0.004	0.046	0.149
INTERFACE UNIT # 2			
Initial	6.500	44.000	-15.000
Final	6.397	40.014	-14.049
Reolution	1.000	1.000	1.000
Standard Deviation	0.005	0.053	0.078

Table-5.2 (x,z) coordinates of the interface units of model M2D1 after inversion of wide angle reflection travel times (units in kms.).

	INTERFACE UNIT # 1		
Initial	9.91,13.65	18.2,14.65	27.5,15.4
Final	10.0,12.50	20.0,15.00	30.0,17.5
	INTERFACE UNIT # 2		
Initial	44.91,22.0	50.07,22.0	55.22,22.0
Final	40.00,20.0	50.00,20.0	60.00,20.0
	INTERFACE UNIT # 3		
Initial	88.87,20.19	94.44,18.70	100.25,17.14
Final	90.00,17.60	100.,15.100	110.00,12.60

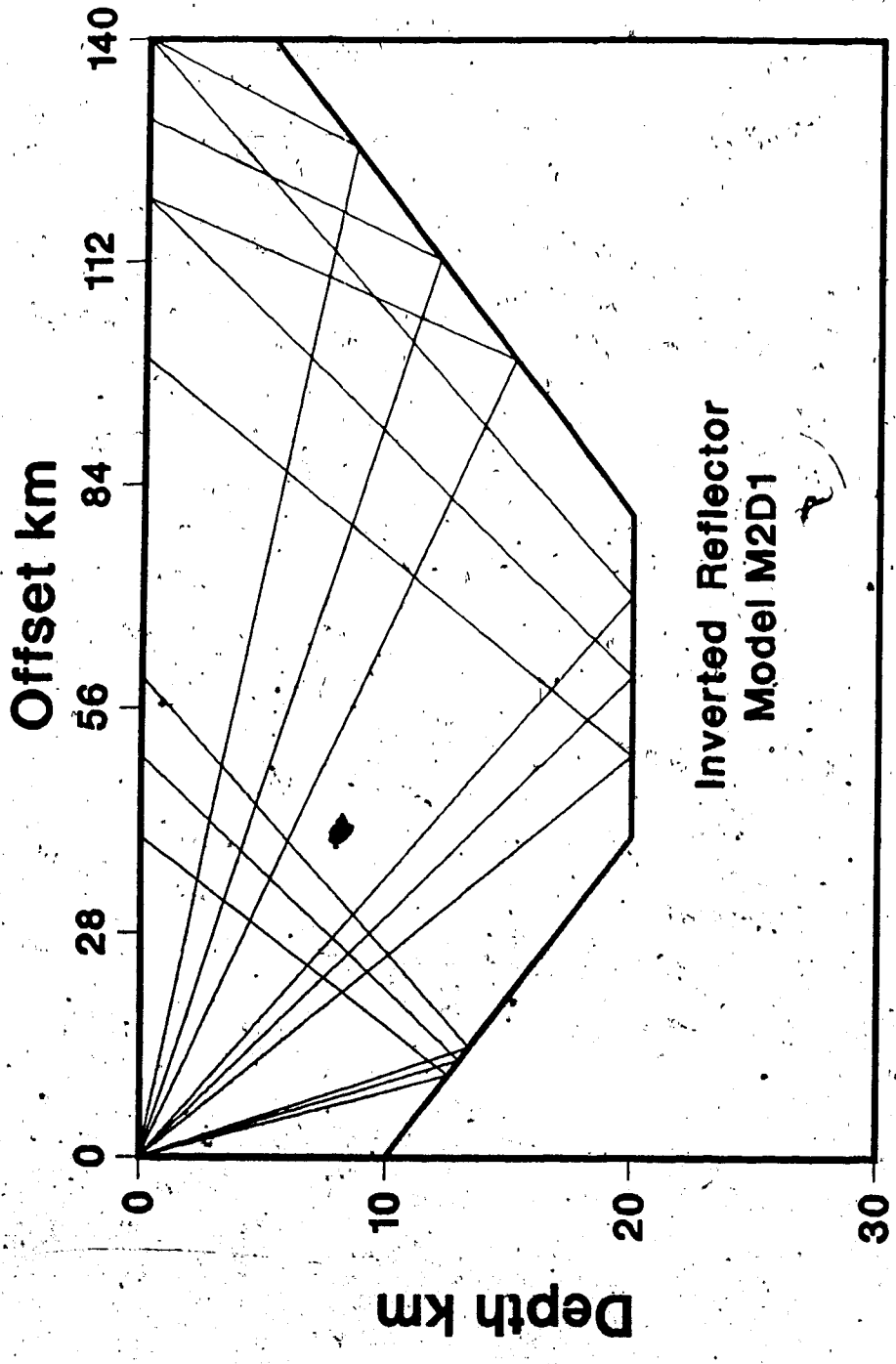

Figure 5.1 Model M2D1: two-layer homogeneous velocity model with arbitrarily dipping reflector boundaries.

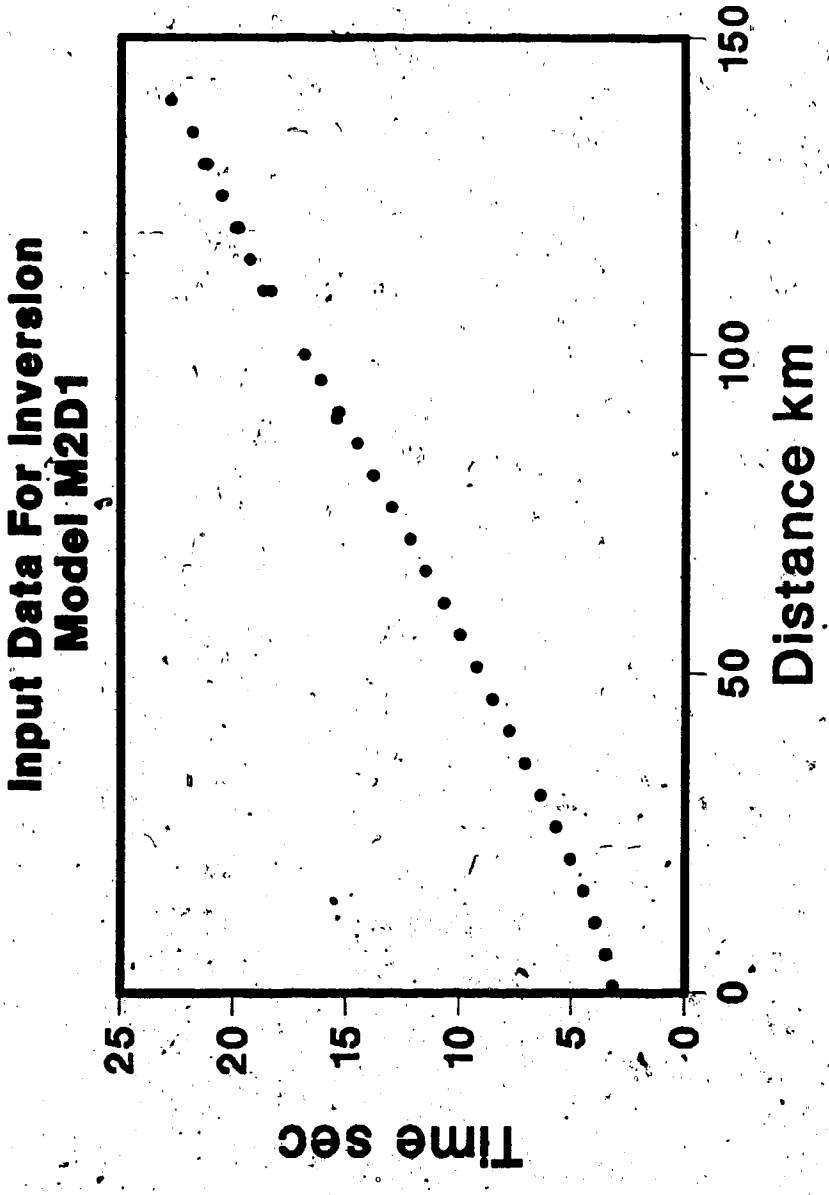

Figure 5.2 Synthetic data generated from forward model calculation of model M2D1.

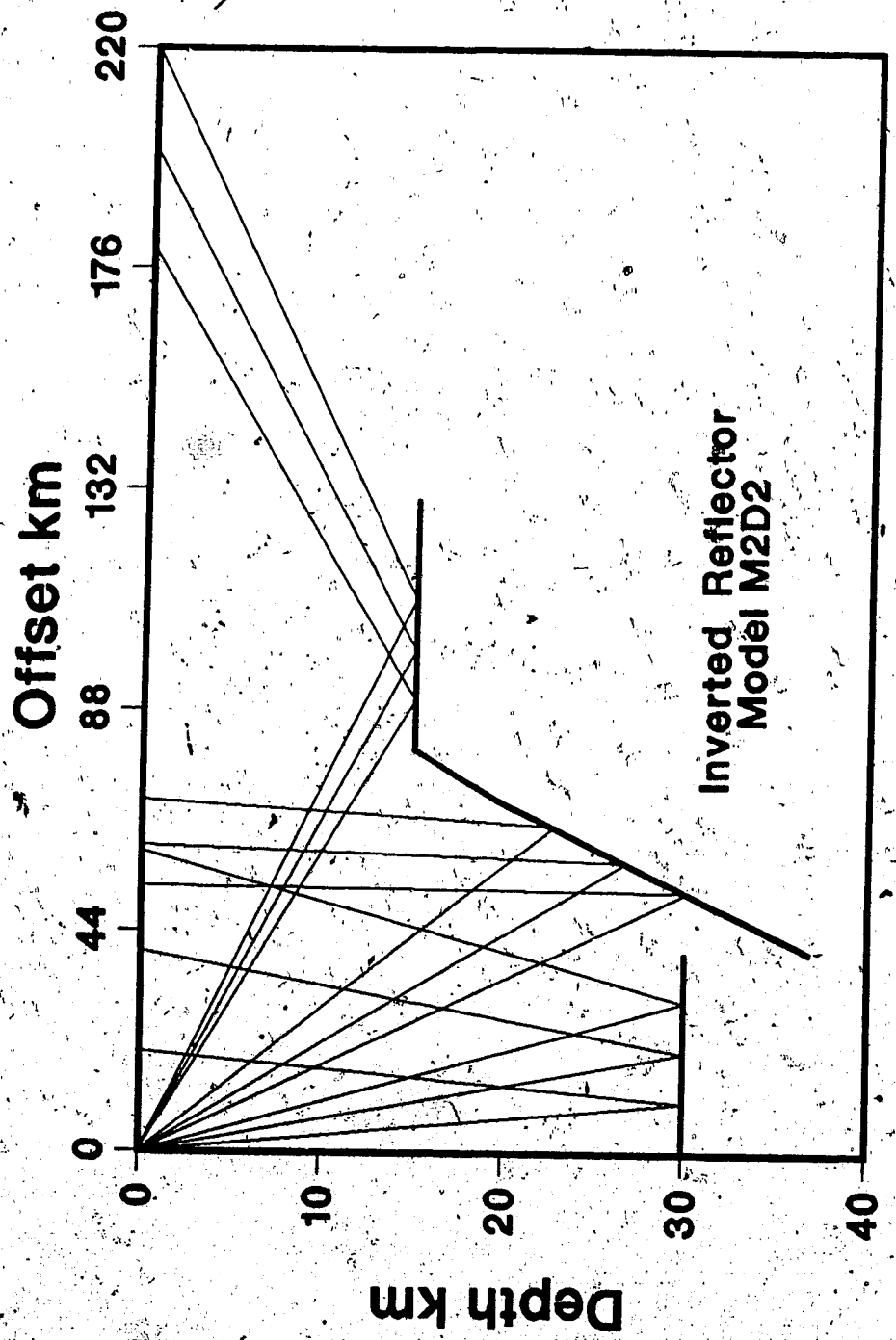

Figure 5.3 Model M2D2: two-layer homogeneous velocity model with arbitrarily dipping reflector boundaries.

The results of inversion from the data set shown in figure-5.4 are listed in tables-5.3 and 5.4.

5.3 Field Examples:

The set of PmP data mentioned in Chapter-4 (see figure-4.8) is again considered here for inversion in terms of a 2-D dipping model. This is done intentionally, to emphasize the suitability of the present method over the curved boundary assumption for this specific case. Every three points in the data space are used to generate a part of the Moho interface. It should be mentioned that the program developed for the 2-D dipping boundaries is only valid for a two-layer model. Usually the Moho boundary is located below several intermediate crustal boundaries. Rays starting from the source at the surface are refracted at these intermediate boundaries before they reach the Moho interface. Similar bending occurs when the reflected rays pass through these boundaries to emerge at the receiver location on the surface. As a result the rays suffer deviation from the straight line paths used in equation (1) with a two-layer assumption. A more general type of forward model should take care of these intermediate refracting boundaries to ensure a more accurate result (to be adopted in future studies). For now the results obtained using a two-layer assumption remain only as approximate ones. This is particularly true for the interface coordinate values. The effect of refraction on the computed average velocity is less prominent. Nonetheless the present algorithm reflects the main features of the inversion process. Figure-5.5,

Table 5.3 Results from iterative inversion of synthetic wide angle reflection times in terms of arbitrarily dipping interface model M2D2.

	Velocity (km/s)	Depth (km)	Dip Angle (deg)
INTERFACE UNIT # 1			
Initial	6.500	33.000	0.000
Final	6.399	29.997	-0.015
Resolution	1.000	1.000	1.000
Standard Deviation	0.001	0.003	0.013
INTERFACE UNIT # 2			
Initial	6.500	66.200	-33.000
Final	6.419	60.341	-29.947
Resolution	1.000	1.000	1.000
Standard Deviation	0.020	0.522	0.138
INTERFACE UNIT # 3			
Initial	6.500	16.000	0.001
Final	6.399	15.238	-0.259
Reolution	1.000	1.000	1.000
Standard Deviation	0.001	0.223	0.278

Table-5.4 (x,z) coordinates of the interface units of model M2D2 after inversion of wide angle reflection travel times (units in kms.).

	INTERFACE UNIT # 1		
Initial	0.80,32.10	17.64,32.10	28.75,32.10
Final	00.0,30.00	10.00,30.00	30.00,30.00
	INTERFACE UNIT # 2		
Initial	68.31,21.84	73.21,18.66	79.67,14.46
Final	40.00,36.90	50.00,31.10	60.00,25.40
	INTERFACE UNIT # 3		
Initial	91.26,16.00	93.80,16.00	96.33,16.00
Final	80.00,15.00	90.00,15.00	100.0,15.00

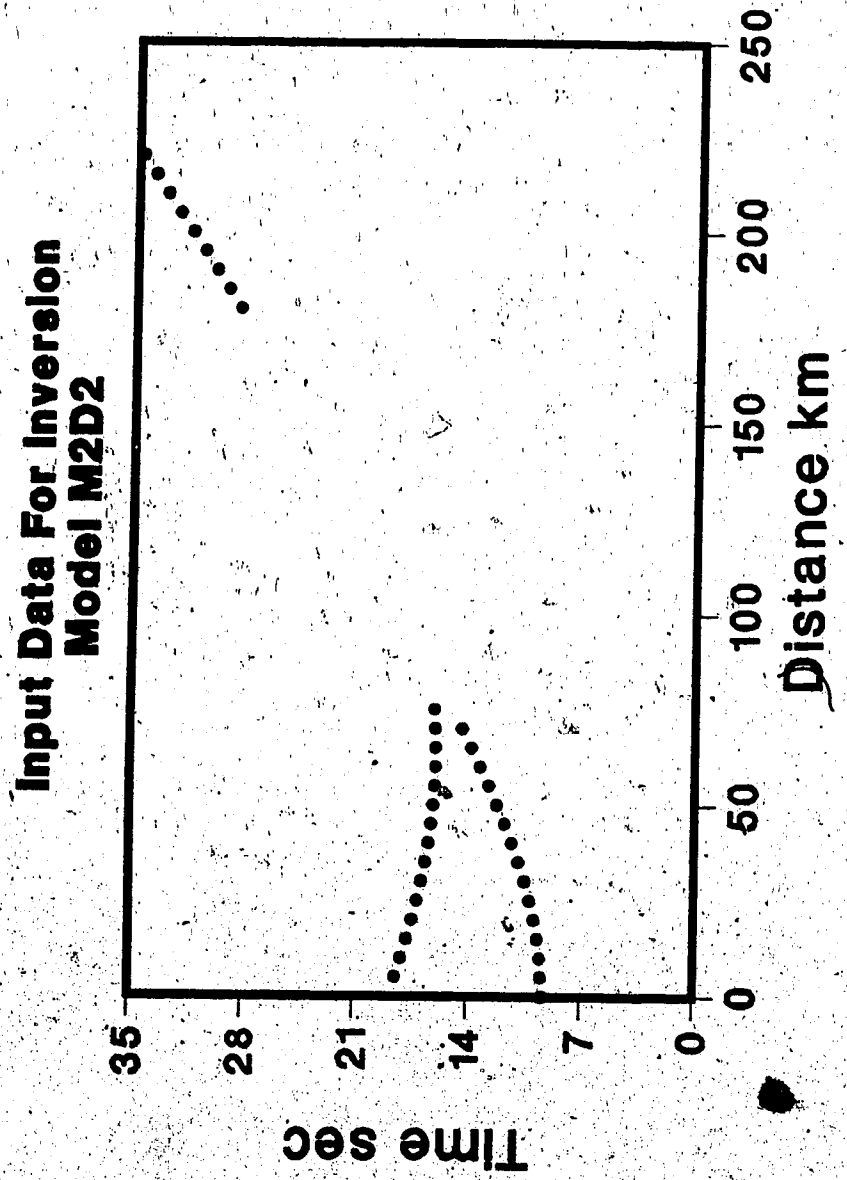

Figure 5.4 Synthetic data generated from forward model calculation of model M2D2.

tables-5.5 and 5.6 include the results of inversion for the observation data mentioned above. The overall RMS value for this inversion is only 0.1 sec.

Finally we include another field example where only the first arrival travel time data are considered. Modeling is done in terms of head waves and dipping boundaries. The forward model for this example is described in Appendix-A4. Data for this field example in southern Saskatchewan were collected by the COCRUST group. An E-W reversed refraction profile approximately 300 km long was shot during two summers of field work in 1979 and 1981. Both direct and reverse profiles containing 72 receiving stations and 2 shot points have been inverted simultaneously in terms of a dipping layer model. Results from the iterative inversion are included in table-5.7. The program converged after 5 iterations. The overall noise RMS value is 0.01 sec which is less than the average travel time picking error of 0.10 second. A standard deviation as large as 2.2 km computed for the thickness of the deepmost layer only indicates lack of observations from the corresponding layer (only 4 observations from Moho in the direct profile). Resolution is extremely good for the top layers. Field data for the direct and reverse refraction profiles are shown in figures-5.6 and 5.7. The inverted model is given in figure-5.8. The results obtained from the field example are in good agreement with the results obtained by Delandro and Moon (1982) from a COCRUST 1977 E-W refraction profile which overlaps the profile under consideration at the eastern end.

Table 5.5 Results from iterative inversion of field wide angle reflection times in terms of arbitrarily dipping interface model.

	Velocity (km/s)	Depth (km)	Dip Angle (rad)
INTERFACE UNIT # 1			
Initial	6.500	45.000	2.000
Final	6.474	49.950	-0.047
Resolution	0.697	0.962	0.848
Standard Deviation	0.151	2.003	0.113
INTERFACE UNIT # 2			
Initial	6.500	45.000	2.000
Final	6.474	38.521	0.085
Resolution	0.700	0.791	0.639
Standard Deviation	0.020	1.762	0.138
INTERFACE UNIT # 3			
Initial	6.500	45.000	2.000
Final	6.474	43.560	0.016
Reolution	0.700	0.804	0.607
Standard Deviation	0.001	1.523	0.118

Table-5.6 Inverted (x,z) coordinates of Moho interface obtained from PmP travel time data shown in figure-4.8 (distance units in kms).

	INTERFACE UNIT # 1		
Initial	60.08,47.10	64.53,47.25	73.06,47.55
Final	71.40,46.51	77.03,46.24	88.11,45.70
	INTERFACE UNIT # 2		
Initial	77.44,47.70	81.04,47.85	83.76,47.93
Final	67.26,44.21	70.61,44.49	72.29,44.64
	INTERFACE UNIT # 3		
Initial	88.5,48.09	91.46,48.19	95.618,48.34
Final	93.8,45.02	97.07,45.06	101.65,45.11

Table-5.7 Results from iterative inversion of COCRUST 1979 & 1981 first arrival travel times (velocity & thickness units are in km/s & km).

Layer	Model parameters	Resolution (diagonal)	Standard Deviation
	P-velocity		
1	3.400	1.00	.05000
2	6.074	1.00	.01400
3	6.487	1.00	.06300
4	6.744	1.00	.04100
5	8.126	1.00	.14100
	Thickness (W)		
1	2.797	1.00	.05600
2	7.393	0.99	1.49002
3	11.431	0.92	1.18020
4	24.007	0.85	2.21000
	Thickness (E)		
1	2.148	1.00	.03200
2	15.500	0.99	1.01000
3	8.067	0.62	1.37000
4	19.367	0.61	1.15000

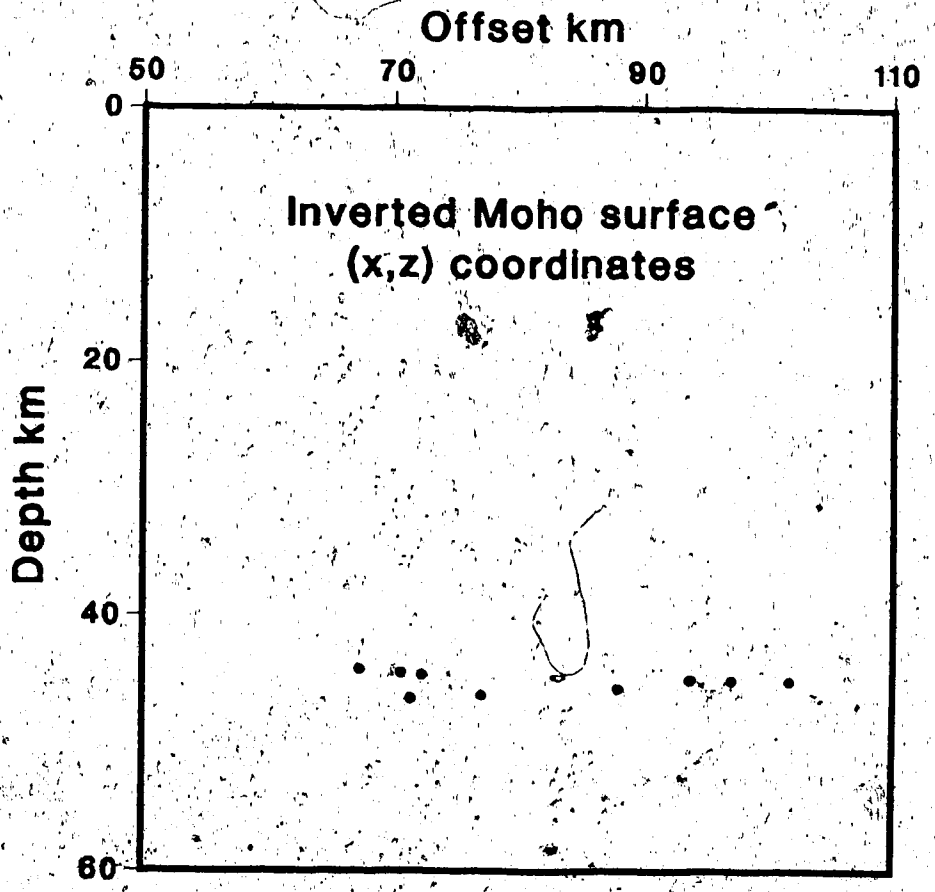

Figure 5.5 Inverted dipping model obtained from wide angle reflection data (line B, South-North, 1979) shown in figure-4.8.

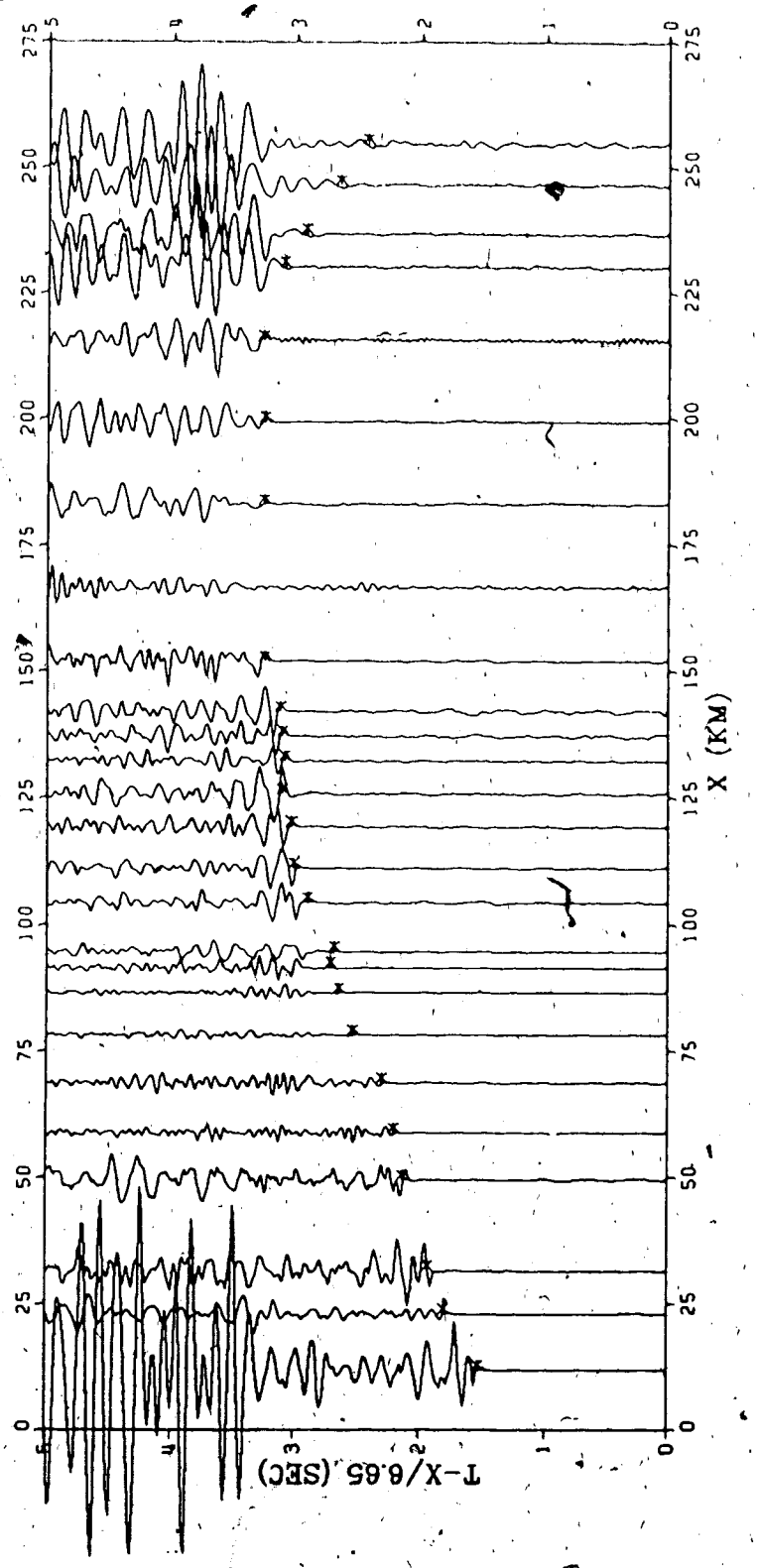

Figure 5.6 First arrival times recorded along the direct profile (COCRUST line C, 1979) in southern Saskatchewan.

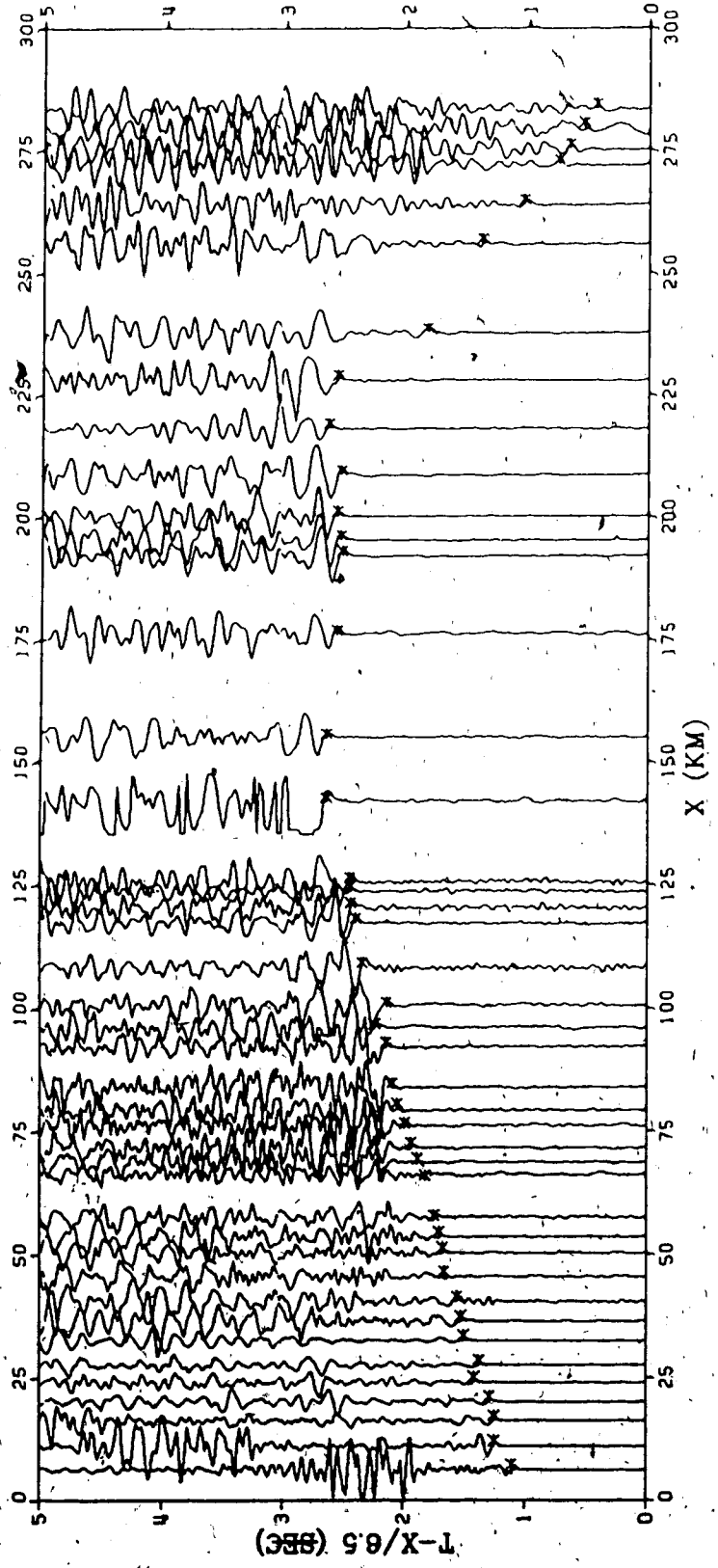

Figure 5.7 First arrival times recorded along the reverse profile (COCRUST line D, 1981) in southern Saskatchewan.

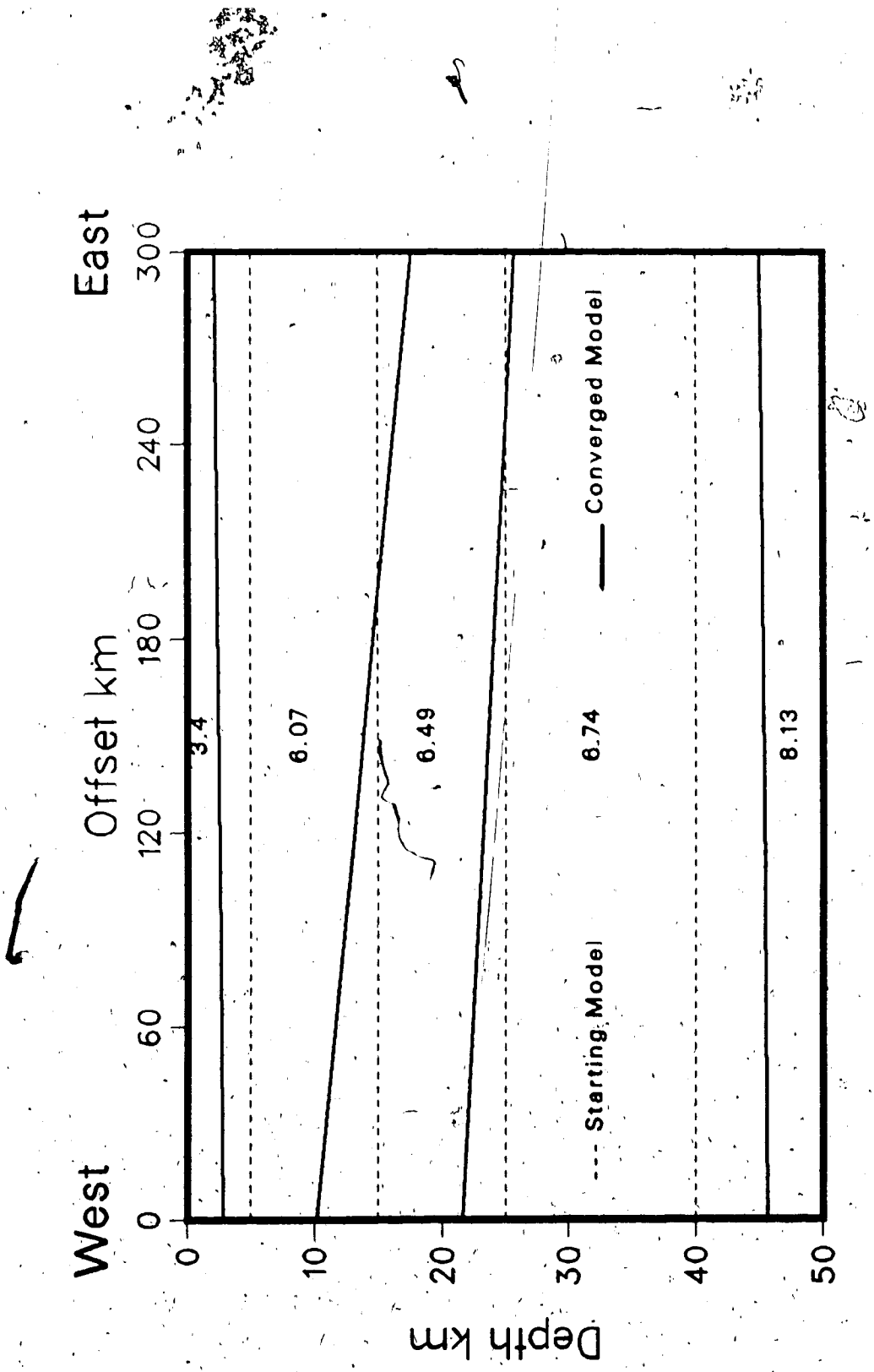

Figure 5.8 Initial and inverted models for field data shown in figures-5.6 & 5.7.

6. SUMMARY

In crustal seismic studies linearized inversion may be considered as an essential tool for data interpretation and modeling. This technique has been proven superior to the conventional forward-methods in many respects. Generally it is able to extract greater or at least equal amount of information from a given data set. It also gives resolution and quantitative error estimates indicating the reliability of the results produced.

It is well known that the interpretation of seismic data remains incomplete without involving the amplitudes. Therefore this study is an important first step towards the use of quantitative amplitude information in seismic modeling. Examples with simple structures indicate the possibility of incorporating complex models in future. Chapters 4 and 5 may be considered as an initial step towards a unified inversion scheme where both travel time and amplitudes are used for relatively complicated structures.

We have shown that:

1. Parameterization of the forward seismic model is convenient using Asymptotic Ray Theory. Useful parameters which contribute actively and effectively to the response function may be selected to reveal important physical properties of the medium under study.
2. Inversion of quantitative amplitude information is possible which is, in principle, a more rigorous and logical approach to seismic interpretation than is the visual waveform matching of synthetic seismograms.

3. Amplitude information in the vertical component seismograms may be used to reveal additional information such as shear wave velocities and densities without referring to the radial component seismograms.
4. The program is efficient in handling multiple layer amplitude data, multiple shot points, multiple reflections and low velocity zones.
5. Mapping of two-dimensional curved reflectors is possible for the inversion of wide angle reflection travel times.
6. Modeling in terms of realistic two-dimensional arbitrarily dipping reflectors is also possible from linearized inversion adopting appropriate forward model calculations.
7. Analytical calculations for the response function and its derivatives were preferred because of their accuracy and speed compared to the numerical calculations.

7. REFERENCES

1. Adachi, R., (1954). "On a proof of fundamental formula concerning refraction method of geophysical prospecting and some remarks", Kumamoto J. Sci., V-2, 18-23.

2. Aki, K. and Richards, P., (1980). Quantitative seismology theory and methods, Vol-2, W. H. Freeman Co., San Franscisco, 522pp.

3. Aki, K., and Lee, W. H. K., (1976). "Determination of three dimensional velocity anomaly under a seismic array using first P-arrival times from local earthquakes, 1. A homogeneous initial model", J. Geo. Res., 81, 4381-4399.

4. Backus, G. E., and Gilbert, J. F., (1967). "The resolving power of gross earth data", Geoph. J. Roy. Astr. Soc., 16, 169-205.

5. Benz, H. M., and Smith, R. B., (1984). "Simultaneous inversion for lateral velocity variations and hypocenter in the Yellowstone region using earthquake and refraction data", J. Geo. Res., 89, 1208-1220.

6. Birch, F., (1964). "Density and composition of mantle and core", J. Geoph. Res., 69, 4377-4387.

7. Braile, L. W., (1973). "Inversion of crustal seismic refraction and reflection data ", J. Geoph. Res., 78, 7738-7744.

8. Cerveny, V., and Ravindra, R., (1971). Theory of seismic head waves, University of Toronto Press, Toronto, 312pp.

9. Chiu, S. K. L., Kanasewich, E. R., and Phadke, S., (1986). "Three dimensional determination of structure and velocity by seismic tomography", Geophysics, 51, 1559-1571.

10. Crosson, R. S., (1976). "Crustal modelling of earthquake data. 1. Simultaneous least squares estimation of hypocenter and velocity parameters", J. Geoph. Res., 81, 3036-3046.

11. Culter, R. T., Bishop, T. N., Wyld, H. W., Shuey, R. T., Kroeger, R. A., Jones, R. C., and Rathbum, M. L., (1984). "Seismic tomography formulation and methodology", Presented at 54th Ann. International Meeting, Soc. Expl. Geoph., Atlanta.

12. Delandro, W., and Moon, W., (1982). "Seismic structure of Superior-Churchill boundary zone", J. Geoph. Res., 87, 6884-6888.

13. Dobrin, M. B., (1976). Introduction to geophysical prospecting., McGraw-Hill Book Co., 207.

14. Forsythe, G. E., Malcom, M. A. and Moler, C. B., (1977). Computer methods for mathematical computations., Prentice-Hall Inc., N. J., 227-235.

15. Garmeny, J.,(1982). "Amplitude constraints in linear inversion of seismic data", J. Geo. Res., 87, 8426-8434.

16. Gersztenkorn, A., Bednar, J. B., and Lines, L. R., (1986). "Robust iterative inversion for the one-dimensional acoustic wave equation", Geophysics, 51, 357-368.

17. Golub, G. H., and Reinsch, C., (1970). Singular value decomposition and least squares solution: Handbook for Automatic Computation, II, Linear algebra, Eds. J. Wilkinson and C Reinsch, Springer-Verlog, Berlin, Heidelberg, New York.

18. Hirahara, K., and Ishikawa, Y., (1984). "Travel time inversion for three-dimensional P-wave velocity anisotropy", J. Phys. Earth, 32, 197-218.

19. Hoerl, A. E., Kennard, R. W., and Baldwin, K. F., (1975). "Ridge regression: some simulations",

Commun. Statist., 4, 105-123.

20. Hoversten, G. M., Dey, A., and Morrison, H. F., (1982). "Comparison of five least-squares inversion techniques in resistivity sounding", Geophys. Prosp., 30, 688-715.

21. Hron, F., Daley, P. F., and Marks, L. W., (1977)."Numerical modelling of seismic body waves in oil exploration and crustal seismology", Comput. Methods in Geoph. Mechanics, 25, 21-42.

22. Ivansson, S., (1985). "A study of methods for tomographic velocity estimation in the presence of low velocity zones", Geophysics, 50, 969-988.

23. Lanczos, C., (1961). Linear Differential Operators., D. Van Nostrand Co., Princeton, 665-679.

24. Lawson, C. L., and Hanson, R. J., (1974). Solving least squares problem, Prentice Hall Inc., New Jersey, 340pp., 1974.

25. Levenberg, K., (1944). "A method for the solution of certain problems in least squares", Quarterly of Appl. Math., 2, 164-168.

26. Lines, L. R., and Treitel, S., (1984). "Tutorial-A

review of least-squares inversion and its application to geophysical problems", Geoph. Prosp., 32, 159-186.

27. Marquardt, D. W., (1963). "An algorithm for least squares estimation of non-linear parameters", J. Soc. Industrial and Appl. Math., 11, 431-441.

28. Marks, L. W., and Hron, F., (1979) "Dynamic properties of reflected and head waves near the critical point", Can. J. Earth Sci., 16, 1388-1401.

29. McNutt, S. R., and Jacob, K. H., (1986) "Determination of large scale velocity structure of the crust and upper mantle in the vicinity of pavlof volcano, Alaska", J. Geo. Res., 91, 5013-5022.

30. Meshbei, V. I., (1968) "Equation of travel time curves for reflected waves of the PS(SP) type and compressional critically diffracted head waves of type P12P21 for a curved surface", Exploration Geophysics, Vol. 47, 45.

31. Mota, L., (1954). "Determination of dips and depths of geological layers by the seismic refraction method". Geophysics, 19, 242-254.

32. Nakanishi, I., (1985). "Three dimensional structure beneath Hokkaido region as derived from a

tomographic inversion of P arrival times", J. Phys. Earth, 33, 241-256.

33. Ursin, B., and Zheng, Y., (1985). "Identification of seismic reflections using singular value decomposition", Geo. Prosp., 33, 773-799.

34. Vignersesse, J. L., (1978). "Damped and constrained least squares method with application to gravity interpretation", J. Geophys, 45, 17-28.

35. Wiggins, R. A., (1972). "The general linear inverse problem. Implications of surface waves and free oscillations for earth structure", Reviews of Geoph. and Space Phys., 10, 251-285.

8. APPENDIX

A1. Derivative of Refraction Coefficient:

$$\frac{\partial R_{13}}{\partial \alpha_1} = 2\rho_1 P_1 D^{-1}(\beta_2 P_2 X + \beta_1 P_4 Y) + 2\alpha_1 \rho_1 D^{-1}(\beta_2 P_2 X + \beta_1 P_4 Y)\frac{\partial P_1}{\partial \alpha_1} - 2\alpha_1 \rho_1 P_1 D^{-2}(\beta_2 P_2 X + \beta_1 P_4 Y)\frac{\partial D}{\partial \alpha_1} \quad (A.1)$$

where,

$$\frac{\partial D}{\partial \alpha_1} = \alpha_2 \beta_1 \beta_2 \theta^2 Z^2 + \beta_1 P_3 P_4 Y^2 + \rho_1 \rho_2 \beta_2 P_2 P_3 + (\alpha_2 \beta_2 P_2 X^2 + \rho_1 \rho_2 \beta_1 \alpha_2 P_4 + q^2 \theta^2 P_2 P_3 P_4)\frac{\partial P_1}{\partial \alpha_1} \quad (A.2)$$

$$\frac{\partial P_1}{\partial \alpha_1} = -\frac{\alpha_1 \theta^2}{P_1} \quad (A.3)$$

$$\frac{\partial R_{13}}{\partial \alpha_2} = -2\alpha_1 \rho_1 P_1 D^{-2}(\beta_2 P_2 X + \beta_1 P_4 Y)\frac{\partial D}{\partial \alpha_2} \quad (A.4)$$

where,

$$\frac{\partial D}{\partial \alpha_2} = \alpha_1 \beta_1 \beta_2 \theta^2 Z^2 + \beta_2 P_1 P_2 X^2 + \rho_1 \rho_2 \beta_1 P_1 P_4 + (\alpha_1 \beta_1 P_4 Y^2 + \rho_1 \rho_2 \alpha_1 \beta_2 P_2 + q^2 \theta^2 P_1 P_2 P_4)\frac{\partial P_3}{\partial \alpha_2} \quad (A.5)$$

$$\frac{\partial P_3}{\partial \alpha_2} = -\frac{\alpha_2 \theta^2}{P_3} \quad (A.6)$$

$$\frac{\partial R_{13}}{\partial \beta_1} = 2\alpha_1 \beta_2 \rho_1 P_1 X D^{-1}\frac{\partial P_2}{\partial \beta_1} + 2\alpha_1 \beta_2 \rho_1 P_1 P_2 D^{-1}\frac{\partial X}{\partial \beta_1} + 2\alpha_1 \rho_1 P_1 P_4 Y D^{-1} + 2\alpha_1 \beta_1 \rho_1 P_1 P_4 D^{-1}\frac{\partial Y}{\partial \beta_1} - 2\alpha_1 \beta_2 \rho_1 P_1 P_2 X D^{-2}\frac{\partial D}{\partial \beta_1} - 2\alpha_1 \beta_1 \rho_1 P_1 P_4 Y D^{-2}\frac{\partial D}{\partial \beta_1} \quad (A.7)$$

where,

$$\frac{\partial P_2}{\partial \beta_1} = -\frac{\beta_1 \theta^2}{P_2} \quad (A.8)$$

$$\frac{\partial X}{\partial \beta_1} = 4\beta_1\rho_1\theta^2 \qquad (A.9)$$

$$\frac{\partial Y}{\partial \beta_1} = -4\beta_1\rho_1\theta^2 \qquad (A.10)$$

where,

$$\frac{\partial D}{\partial \beta_1} = \alpha_1\alpha_2\beta_2\theta^2 Z^2 + \alpha_1 P_3 P_4 Y^2 + \rho_1\rho_2\alpha_2 P_1 P_4 + \alpha_2\beta_2 P_1 P_2\frac{\partial X^2}{\partial \beta_1} + \alpha_1\beta_2 P_3 P_4\frac{\partial Y^2}{\partial \beta_1} + \alpha_1\alpha_2\beta_1\beta_2\theta^2\frac{\partial Z^2}{\partial \beta_1} + (\alpha_1\beta_2\rho_1\rho_2 P_3 + \theta^2 q^2 P_1 P_3 P_4)\frac{\partial P_2}{\partial \beta_1} + \theta^2 P_1 P_2 P_3 P_4\frac{\partial q^2}{\partial \beta_1} \qquad (A.11)$$

$$\frac{\partial X^2}{\partial \beta_1} = 8X\beta_1\rho_1\theta^2 \qquad (A.12)$$

$$\frac{\partial Y^2}{\partial \beta_1} = -8Y\beta_1\rho_1\theta^2 \qquad (A.13)$$

$$\frac{\partial Z^2}{\partial \beta_1} = 8Z\beta_1\rho_1\theta^2 \qquad (A.14)$$

$$\frac{\partial q^2}{\partial \beta_1} = -8Z\beta_1\rho_1 q \qquad (A.15)$$

$$\frac{\partial R_{13}}{\partial \beta_2} = (2\alpha_1\rho_1 P_1 P_2 X + 2\alpha_1\beta_2\rho_1 P_1 P_2\frac{\partial X}{\partial \beta_2} + 2\alpha_1\beta_1\rho_1 P_1 Y\frac{\partial P_4}{\partial \beta_2} + 2\alpha_1\beta_1\rho_1 P_1 P_4\frac{\partial Y}{\partial \beta_2})D^{-1} + (2\alpha_1\beta_2\rho_1 P_1 P_2 X \pm 2\alpha_1\beta_1\rho_1 P_1 P_4 Y)\frac{\partial D^{-1}}{\partial \beta_2} \qquad (A.16)$$

where,

$$\frac{\partial X}{\partial \beta_2} = -4\rho_2\beta_2 P\theta^2 \qquad (A.17)$$

$$\frac{\partial Y}{\partial \beta_2} = 4\rho_2\beta_2 P\theta^2 \qquad (A.18)$$

$$\frac{\partial P_4}{\partial \beta_2} = -\frac{\beta_2\theta^2}{P_4} \qquad (A.19)$$

$$\frac{\partial D}{\partial \beta_2} = \alpha_1\alpha_2\beta_1\theta^2 Z^2 + \alpha_1 P_1 P_2 X^2 + \rho_1\rho_2\alpha_1 P_2 P_3$$

$$+ \alpha_2\beta_2 P_1 P_2 \frac{\partial X^2}{\partial \beta_2} + \alpha_1\beta_1 P_3 P_4 \frac{\partial Y^2}{\partial \beta_2} + \alpha_1\alpha_2\beta_1\beta_2\theta^2 \frac{\partial Y^2}{\partial \beta_2}$$
$$+ (\alpha_1\beta_1 P_3 Y^2 + \rho_1\rho_2 P_3\theta^2 q^2 + \alpha_2\beta_1\rho_1\rho_2 P_1)\frac{\partial P_4}{\partial \beta_2}$$
$$+ P_1 P_2 P_3 P_4 \theta^2 \frac{\partial q^2}{\partial \beta_2} \qquad (A.20)$$

where,

$$\frac{\partial X^2}{\partial \beta_2} = -8X\beta_2\rho_2\theta^2 \qquad (A.21)$$

$$\frac{\partial Y^2}{\partial \beta_2} = 8Y\beta_2\rho_2\theta^2 \qquad (A.22)$$

$$\frac{\partial Z^2}{\partial \beta_2} = -8Z\beta_2\rho_2\theta^2 \qquad (A.23)$$

$$\frac{\partial q^2}{\partial \beta_2} = 8\beta_2\rho_2 q \qquad (A.24)$$

$$\frac{\partial R_{1,4}}{\partial \rho_1} = (2\alpha_1\beta_2 P_1 P_2 X + 2\alpha_1\beta_2\rho_1 P_1 P_2 \frac{\partial X}{\partial \rho_1}$$
$$+ 2\alpha_1\beta_1 P_1 P_4 Y + 2\alpha_1\beta_1\rho_1 P_1 P_4 \frac{\partial Y}{\partial \rho_1})D^{-1}$$
$$+ (2\alpha_1\beta_2\rho_1 P_1 P_2 X + 2\alpha_1\beta_1\rho_1 P_1 P_4 Y)\frac{\partial D^{-1}}{\partial \rho_1} \qquad (A.25)$$

where,

$$\frac{\partial X}{\partial \rho_1} = 2\beta_1^2\theta^2 \qquad (A.26)$$

$$\frac{\partial Y}{\partial \rho_1} = 1 - 2\beta_1^2\theta^2 \qquad (A.27)$$

$$\frac{\partial D}{\partial \rho_1} = \alpha_1\beta_2\rho_2 P_2 P_3 + \alpha_2\beta_1\rho_2 P_1 P_4 + \alpha_2\beta_2 P_1 P_2 \frac{\partial X^2}{\partial \rho_1}$$
$$+ \alpha_1\beta_1 P_3 P_4 \frac{\partial Y^2}{\partial \rho_1} + \alpha_1\alpha_2\beta_1\beta_2\theta^2 \frac{\partial Z^2}{\partial \rho_1} + \theta^2 P_1 P_2 P_3 P_4 \frac{\partial q^2}{\partial \rho_1} \qquad (A.28)$$

$$\frac{\partial X^2}{\partial \rho_1} = 4X\beta_1^2\theta^2 \qquad (A.29)$$

$$\frac{\partial Y^2}{\partial \rho_1} = 2Y(1 - 2\beta_1^2\theta^2) \qquad (A.30)$$

$$\frac{\partial Z^2}{\partial \rho_1} = 2Z(-1 + 2\beta_1^2\theta^2) \qquad (A.31)$$

$$\frac{\partial q^2}{\partial \rho_1} = -8q\beta_1^2 \qquad (A.32)$$

$$\frac{\partial R_{13}}{\partial \rho_2} = (2\alpha_1\beta_2\rho_1 P_1 P_2 X + 2\alpha_1\beta_1\rho_1 P_1 P_4 Y)\frac{\partial D^{-1}}{\partial \rho_2} + (2\alpha_1\beta_1\rho_1 P_1 P_4 \frac{\partial Y}{\partial \rho_2} + 2\alpha_1\beta_2\rho_1 P_1 P_2 \frac{\partial X^2}{\partial \rho_1})D^{-1} \qquad (A.33)$$

where,

$$\frac{\partial X}{\partial \rho_2} = 1 - 2\beta_2^2\theta^2 \qquad (A.34)$$

$$\frac{\partial Y}{\partial \rho_2} = 2\beta_2^2\theta^2 \qquad (A.35)$$

$$\frac{\partial D}{\partial \rho_2} = \alpha_1\beta_2\rho_1 P_2 P_3 + \alpha_2\beta_1\rho_1 P_1 P_4 + \alpha_2\beta_2 P_1 P_2 \frac{\partial X^2}{\partial \rho_2} + \alpha_1\beta_1 P_3 P_4 \frac{\partial Y^2}{\partial \rho_2} + \alpha_1\alpha_2\beta_1\beta_2\theta^2 \frac{\partial Z^2}{\partial \rho_2} + \theta^2 P_1 P_2 P_3 P_4 \frac{\partial q^2}{\partial \rho_2} \qquad (A.36)$$

$$\frac{\partial X^2}{\partial \rho_2} = 2X(1 - 2\beta_2^2\theta^2) \qquad (A.37)$$

$$\frac{\partial Y^2}{\partial \rho_2} = 4Y\beta_2^2\theta^2) \qquad (A.38)$$

$$\frac{\partial Z^2}{\partial \rho_2} = 2Z(1 - 2\beta_2^2\theta^2) \qquad (A.39)$$

$$\frac{\partial q^2}{\partial \rho_1} = 4q\beta_2^2 \qquad (A.40)$$

A2. Derivatives of Reflection Coefficient:

$$\frac{\partial R_{11}}{\partial \alpha_1} = 2\frac{\partial P_1}{\partial \alpha_1}\{(\alpha_2\beta_2 P_2 X^2 + \alpha_2\beta_1\rho_1\rho_2 P_4 + q^2\theta^2 P_2 P_3 P_4)D^{-1}\}$$

$$+ 2P_1(\alpha_2\beta_2P_2X^2 + \alpha_2\beta_1\rho_1\rho_2P_4 + q^2\theta^2P_2P_3P_4)D^{-1}\frac{\partial D^{-1}}{\partial \alpha_1} \tag{A.41}$$

$$\frac{\partial \mathcal{R}_{11}}{\partial \alpha_2} = 2P_1D^{-1}(\beta_2P_2X^2 + \beta_1\rho_1\rho_2P_4 + q^2\theta^2P_2P_4\frac{\partial P_3}{\partial \alpha_2}) + 2P_1(\alpha_2\beta_2P_2X^2 + \alpha_2\beta_1\rho_1\rho_2P_4 + q^2\theta^2P_3P_4)\frac{\partial D^{-1}}{\partial \alpha_2} \tag{A.42}$$

$$\frac{\partial \mathcal{R}_{11}}{\partial \beta_1} = 2P_1D^{-1}(\alpha_2\beta_2\frac{\partial P_2}{\partial \beta_1}X^2 + \alpha_2\beta_2P_2\frac{\partial X^2}{\partial \beta_1} + \alpha_2\rho_1\rho_2P_4 + q^2\theta^2P_3P_4)\frac{\partial P_2}{\partial \beta_1} + \frac{\partial q^2}{\partial \beta_1}\theta^2P_3P_4) + 2P_1(\alpha_2\beta_2P_2X^2 + \alpha_2\beta_1\rho_1\rho_2P_4 + q^2\theta^2P_3P_4)\frac{\partial D^{-1}}{\partial \beta_1} \tag{A.43}$$

$$\frac{\partial \mathcal{R}_{11}}{\partial \beta_2} = 2P_1D^{-1}(\alpha_2P_2X^2 + \alpha_2\beta_2P_2\frac{\partial X^2}{\partial \beta_2} + \beta_1\alpha_2\rho_1\rho_2\frac{\partial P_4}{\partial \beta_2} + \theta^2P_3P_4\frac{\partial q^2}{\partial \beta_2} + q^2\theta^2P_3P_4)\frac{\partial P_4}{\partial \beta_2} + 2P_1(\alpha_2\beta_2P_2X^2 + \alpha_2\beta_1\rho_1\rho_2P_4 + q^2\theta^2P_3P_4)\frac{\partial D^{-1}}{\partial \beta_2} \tag{A.44}$$

$$\frac{\partial \mathcal{R}_{11}}{\partial \rho_1} = 2P_1D^{-1}(\alpha_2\beta_2P_2\frac{\partial X^2}{\partial \rho_1} + \beta_1\alpha_2\rho_2P_4 + \theta^2P_2P_3P_4\frac{\partial q^2}{\partial \rho_1}) + 2P_1(\alpha_2\beta_2P_2X^2 + \alpha_2\beta_1\rho_1\rho_2P_4 + q^2\theta^2P_3P_4)\frac{\partial D^{-1}}{\partial \rho_1} \tag{A.45}$$

$$\frac{\partial \mathcal{R}_{11}}{\partial \rho_2} = 2P_1D^{-1}(\alpha_2\beta_2P_2\frac{\partial X^2}{\partial \rho_2} + \beta_1\alpha_2\rho_1P_4 + \theta^2P_2P_3P_4\frac{\partial q^2}{\partial \rho_2}) + 2P_1(\alpha_2\beta_2P_2X^2 + \alpha_2\beta_1\rho_1\rho_2P_4 + q^2\theta^2P_3P_4)\frac{\partial D^{-1}}{\partial \rho_2} \tag{A.46}$$

A3. Derivatives of Amplitude:

Amplitude function in terms of reflection coefficient and geometrical spreading can be written as

$$A = \frac{\eta R}{L}$$

where,

η = unit vector tangent to the last ray segment.

L = geometrical spreading.

$R = \mathcal{R}_{12}\mathcal{R}_{21}\mathcal{R}_{23}\mathcal{R}_{32}\mathcal{R}_{33}$ (3-layer case for example)

$$\frac{\partial A}{\partial \alpha_1} = \frac{N}{L}\frac{\partial R}{\partial \alpha_1} - \frac{NR}{L^2}\frac{\partial L}{\partial \alpha_1} + \frac{N}{L}\frac{\partial N}{\partial \alpha_1}$$

$$\frac{\partial A}{\partial \alpha_2} = \frac{N}{L}\frac{\partial R}{\partial \alpha_2} - \frac{NR}{L^2}\frac{\partial L}{\partial \alpha_2} + \frac{N}{L}\frac{\partial N}{\partial \alpha_2}$$

$$\frac{\partial A}{\partial \alpha_3} = \frac{N}{L}\frac{\partial R}{\partial \alpha_3}$$

$$\frac{\partial A}{\partial \beta_1} = \frac{N}{L}\frac{\partial R}{\partial \beta_1}$$

$$\frac{\partial A}{\partial \beta_2} = \frac{N}{L}\frac{\partial R}{\partial \beta_2}$$

$$\frac{\partial A}{\partial \beta_3} = \frac{N}{L}\frac{\partial R}{\partial \beta_3}$$

$$\frac{\partial A}{\partial \rho_1} = \frac{N}{L}\frac{\partial R}{\partial \beta_1}$$

$$\frac{\partial A}{\partial \rho_2} = \frac{N}{L}\frac{\partial R}{\partial \beta_2}$$

$$\frac{\partial A}{\partial \rho_3} = \frac{N}{L}\frac{\partial R}{\partial \beta_3}$$

$$\frac{\partial R}{\partial \alpha_1} = \frac{\partial R_{12}}{\partial \alpha_1} R_{21} R_{23} R_{32} R_{33} + R_{12}\frac{\partial R_{21}}{\partial \alpha_1} R_{23} R_{32} R_{33} \qquad (A.47)$$

and so on....

A4. Calculation of Travel Time for Dipping Layer:

The dipping layer model considered for the inversion of field travel time data in Chapter-5 has been given by Adachi (1954). The travel time expression for the direct profile (figure-8.1) in case of an n-layer model is given by

$$T_{AB} = \sum_{i=1}^{n-1} (Z_{iA}\cos\alpha_{in} + Z_{iB}\cos\beta_{in})/V_i$$
$$+ X_{AB}\cos\theta_1\cos(\theta_2-\theta_1)\ ..\cos(\theta_{n-1}-\theta_{n-2})/V_n \qquad (A.48)$$

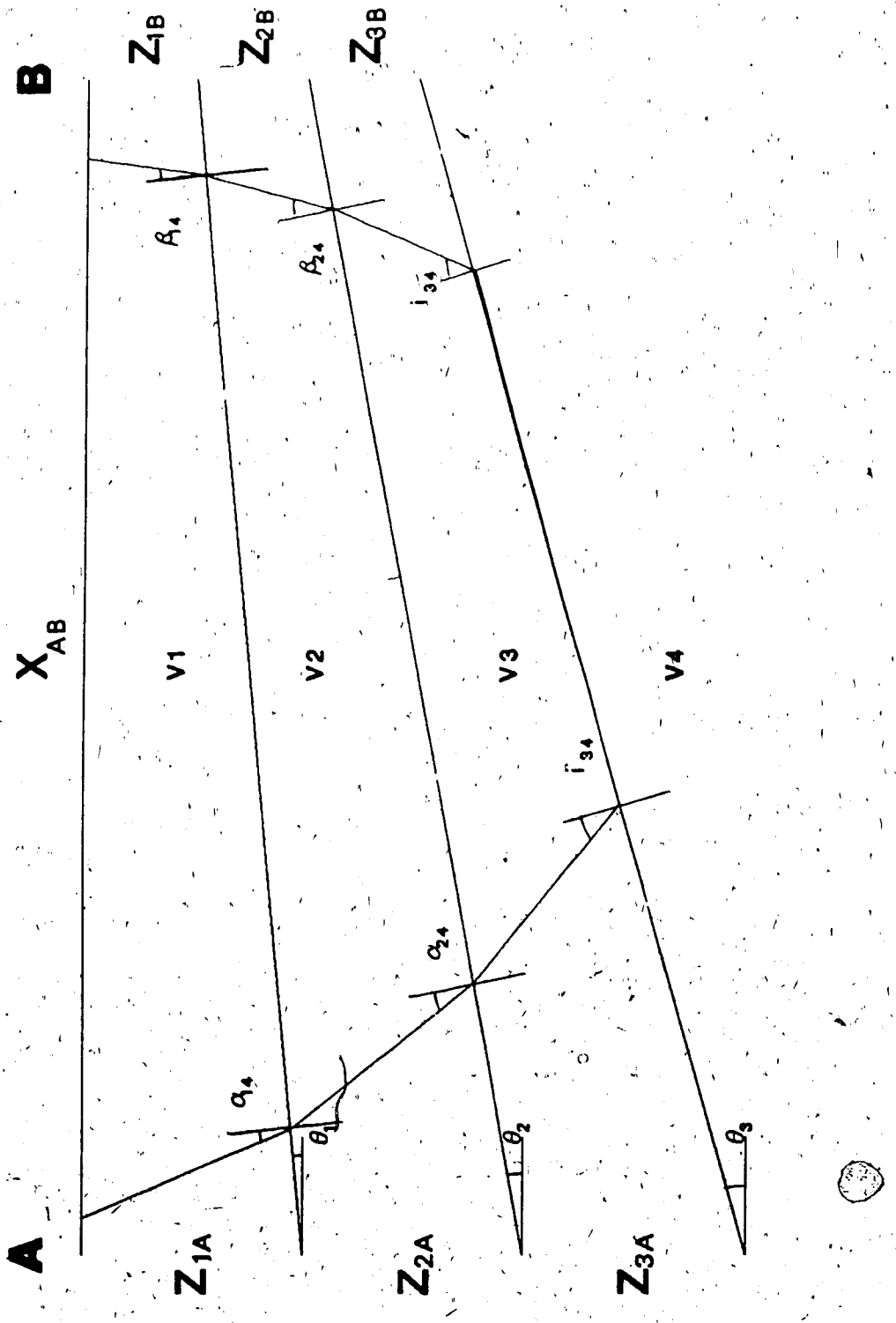

Figure 8.1 Model with ray path parameters used in the derivation of travel time expression A.48.

A5. Derivation of Normal Equations:

$E = A\Delta X - \Delta B$

E^tE

$= (A\Delta X - \Delta B)^t(A\Delta X - \Delta B)$

$= (\Delta X^tA^t - \Delta B^t)(A\Delta X - \Delta B)$

$= \Delta X^tA^tA\Delta X - \Delta X^tA^t\Delta B - \Delta B^tA\Delta X + \Delta B^t\Delta B$

$\partial E^tE/\partial\Delta X = \Delta X^tA^tA - \Delta B^tA = 0$

i.e., $\Delta X^tA^tA = \Delta B^tA$

$A^tA\Delta X = A^t\Delta B$ (A.49)

which is the normal equation (called normal since $A^t(A\Delta X - \Delta B)=0$).

Normal equation with constraint:

If E^tE is minimized subject to constraint $\Delta X^t\Delta X = \Delta X_o^2$

$\frac{\partial}{\partial\Delta X}[E^tE + \beta(\Delta X^t\Delta X - \Delta X_o^2)] = 0$

i.e., $\Delta X^tA^tA - \Delta B^tA + \beta\Delta X^t = 0$

$\Delta X^t(A^tA + \beta I) = \Delta B^tA$

$(A^tA + \beta I)\Delta X = A^t\Delta B$ (A.50)

Using Singular Value Decomposition for the matrix A we get $A = U\Lambda V^t$ and $A^t = V\Lambda U^t$. Therefore we can write

$A^tA + \beta I$

$= V\Lambda U^tU\Lambda V^t + \beta I$

$= V\Lambda^2V^t + \beta I$

$= V(\Lambda^2 + \beta I)V^t$

Therefore,

$$(A^tA + \beta I)^{-1} = V(\Lambda^2 + \beta I)^{-1}V^t \qquad (A.51)$$

From equations(A.50) and (A.51) we can write

$$\begin{aligned}\Delta X &= (A^tA + \beta I)^{-1}A^t\Delta B \\ &= V(\Lambda^2 + \beta I)^{-1}V^tV\Lambda U^t\Delta B \\ &= V(\Lambda^2 + \beta I)^{-1}\Lambda U^t\Delta B \qquad (A.52)\end{aligned}$$

A6. Derivatives of Geometrical Spreading:

$$\begin{aligned}\frac{\partial L}{\partial \alpha_1} &= \frac{\partial}{\partial \alpha_1}\left(\frac{2}{v_1}\right)\cos\theta_1 \sum_{j=1}^{s}(h_jv_j/\cos\theta_j)^{1/2} \sum_{j=1}^{s}(h_jv_j/\cos^3\theta_j)^{1/2} \\ &+ \frac{2}{v_1}\frac{\partial\cos\theta_1}{\partial\alpha_1}\sum_{j=1}^{s}(h_jv_j/\cos\theta_j)^{1/2} \sum_{j=1}^{s}(h_jv_j/\cos^3\theta_j)^{1/2} \\ &+ \frac{2\cos\theta_1}{v_1}\frac{\partial}{\partial\alpha_1}\left[\sum_{j=1}^{s}(h_jv_j/\cos\theta_j)^{1/2}\right] \sum_{j=1}^{s}(h_jv_j/\cos^3\theta_j)^{1/2} \\ &+ \frac{2\cos\theta_1}{v_1}\sum_{j=1}^{s}(h_jv_j/\cos\theta_j)^{1/2}\frac{\partial}{\partial\alpha_1}\left[\sum_{j=1}^{s}(h_jv_j/\cos^3\theta_j)^{1/2}\right]\end{aligned}$$

$$\frac{\partial\cos\theta_1}{\partial\alpha_1} = \frac{\partial}{\partial\alpha_1}(1 - p^2\alpha_1^2)^{-1/2} = -v_1p^2(1 - p^2v_1^2)^{-1/2}$$

$$\begin{aligned}&\frac{\partial}{\partial\alpha_1}\sum_{j=1}^{s}(h_jv_j/\cos\theta_j) \\ &= \frac{\partial}{\partial\alpha_1}\left(\frac{v_1h_1}{\cos\theta_1} + \frac{v_2h_2}{\cos\theta_2} + \ldots\right) \\ &= \frac{h_1}{\cos\theta_1} + v_1h_1\frac{\partial}{\partial\alpha_1}\left(\frac{1}{\cos\theta_1}\right) \\ &= \frac{h_1}{\cos\theta_1} + \frac{v_1^2p^2h_1}{\cos\theta_1^3}\end{aligned}$$

$$\frac{\partial}{\partial \alpha_1}\left(\frac{v_1 h_1}{\cos\theta_1^3} + \frac{v_2 h_2}{\cos\theta_2^3} + \ldots\right)$$

$$= \frac{h_1}{\cos\theta_1^3} + \frac{3v_1^2 p^2 h_1}{\cos\theta_1^5}$$

where,

$$\frac{\sin\theta_2}{v_2} = p$$

$$\cos\theta_2 = (1 - v_2^2 p^2)^{1/2}$$

$$\frac{\partial \sin\theta_2}{\partial v_2} = - \frac{v_2 p^2}{\cos\theta_2}$$

$$\frac{\partial}{\partial v_2}\left(\frac{1}{\cos\theta_2}\right)$$

$$= \frac{v_2 p^2}{\cos\theta_2^3}$$

$$\frac{\partial \sin\theta_2}{\partial v_2} = \frac{3 v_2 p^2}{\cos\theta_2^5}$$

$$\frac{\partial L}{\partial \alpha_n} = 0$$

$$\frac{\partial L}{\partial \beta_i} = 0$$

$$\frac{\partial L}{\partial \rho_i} = 0$$

A.7 Calculation of (x,z) coordinates of ray-boundary intersection:

Figure-8.2 shows the reflected ray from a dipping boundary. The following notations are used

AB, BC = incident and reflected ray paths.

θ_1, θ_2 = incident and reflected angles.

m = tangent of the slope angle of the boundary.

X_m = AC = shot-receiver distance.

Z_o = depth of the boundary below the shot point.

From triangles ΔADB and ΔBCF respectively we can write

$$\frac{AD}{\sin\theta_1} = \frac{AB}{\sin D}$$

$$\frac{CF}{\sin(180-\theta_2)} = \frac{BC}{\sin F}$$

But equality of incident and reflection angles requires

$\theta_1 = \theta_2$

$$AB + BC = AD\frac{\sin D}{\sin\theta_1} + CF\frac{\sin F}{\sin\theta_2}$$

$$AB + BC = \frac{1}{\sin\theta_1}(AD\sin D + CF\sin F)$$

$\sin F = \sin D$

$$AB + BC = \frac{\sin D}{\sin\theta_1}(AD + CF)$$

$$= \frac{\sin D}{\sin\theta_1}(Z_o + Z_o + mX_m)$$

where, $CF = Z_o + mX_m$.

$$AB + BC = \frac{AB}{AD}(2Z_o + mX_m)$$

$$AB + BC = AB(2 + mX_m/Z_o)$$

$$= (x^2 + z^2)^{1/2}(2 + mX_m/Z_o)$$

where $AB = (x^2 + z^2)$

$z = Z_o + mx$

$BC = [(x-X_m)^2 + z^2]^{1/2}$

The path length (AB + BC) is also calculated from

$$AB + BC = VT \qquad (A.54)$$

where,

V = Upper medium velocity.

T = Time spent by the ray along path sections AB and BC.

Solution of equations A.53 and A.54 can be obtained in

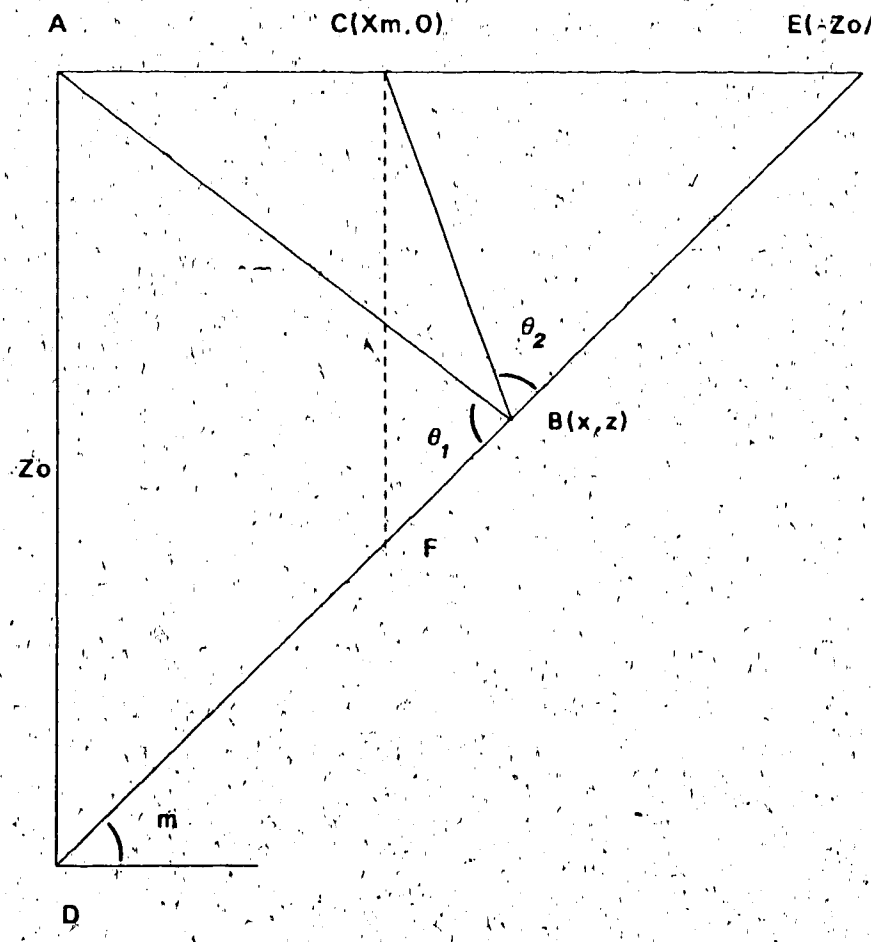

Figure 8.2 Sketch of reflected ray from a dipping boundary.

terms of (x,z) coordinates by adopting a suitable numerical method.